Aqueous SOA formation from the direct photosensitized oxidation of vanillin in the absence and presence of ammonium nitrate

Beatrix Rosette Go Mabato[1], Yan Lyu[1], Yan Ji[1], Yong Jie Li[2], Dan Dan Huang[3], Xue Li[4], Theodora Nah[1], Chun Ho Lam[1], and Chak K. Chan[1]*

[1]School of Energy and Environment, City University of Hong Kong, Hong Kong, China
[2]Department of Civil and Environmental Engineering, and Centre for Regional Ocean, Faculty of Science and Technology, University of Macau, Macau, China
[3]Shanghai Academy of Environmental Sciences, Shanghai 200233, China
[4]Institute of Mass Spectrometry and Atmospheric Environment, Jinan University No. 601 Huangpu Avenue West, Guangzhou 510632, China

Correspondence to: Chak K. Chan (Chak.K.Chan@cityu.edu.hk)

Abstract. Vanillin (VL), a phenolic aromatic carbonyl abundant in biomass burning emissions, forms triplet excited states (^{3}VL*) under simulated sunlight leading to aqueous secondary organic aerosol (aqSOA) formation. Nitrate and ammonium are among the main components of biomass burning aerosols and cloud/fog water. Under atmospherically relevant cloud and fog conditions, solutions composed of either VL only or VL with ammonium nitrate were subjected to simulated sunlight irradiation to compare aqSOA formation via the direct photosensitized oxidation of VL in the absence and presence of ammonium nitrate. The reactions were characterized by examining the VL decay kinetics, product compositions, and light absorbance changes. Both conditions generated oligomers, functionalized monomers, and oxygenated ring-opening products, and ammonium nitrate promoted functionalization and nitration, likely due to its photolysis products ($^•$OH, $^•$NO$_2$, and NO$_2^-$ or HONO). Moreover, a potential imidazole derivative observed in the presence of ammonium nitrate suggested that ammonium participated in the reactions. The majority of the most abundant products from both conditions were potential Brown carbon (BrC) chromophores. The effects of oxygen (O$_2$), pH, and reactants concentration and molar ratios on the reactions were also explored. Our findings show that O$_2$ plays an essential role in the reactions, and oligomer formation was enhanced at pH < 4. Also, functionalization was dominant at low VL concentration, whereas oligomerization was favored at high VL concentration. Furthermore, oligomers and hydroxylated products were detected from the oxidation of guaiacol (a non-carbonyl phenol) via VL photosensitized reactions. Lastly, potential aqSOA formation pathways via the direct photosensitized oxidation of VL in the absence and presence of ammonium nitrate were proposed. This study indicates that the direct photosensitized oxidation of VL may be an important aqSOA source in areas influenced by biomass burning and underscores the importance of nitrate in the aqueous-phase processing of aromatic carbonyls.

1 Introduction

Aqueous reactions can be an important source of secondary organic aerosols (SOA) (Blando and Turpin, 2000; Volkamer et al., 2009; Lim et al., 2010; Ervens et al., 2011; Huang et al., 2011; Lee et al., 2011; Smith et al., 2014) such as highly-oxygenated and low-volatility organics (Hoffmann et al., 2018; Liu et al., 2019) which may affect aerosol optical properties due to contributions to Brown Carbon (BrC) (Gilardoni et al., 2016). BrC refers to organic aerosols that absorb radiation efficiently in the near-ultraviolet (UV) and visible regions (Laskin et al., 2015). The formation of aqueous SOA (aqSOA) via photochemical reactions involves oxidation, with hydroxyl radical ($^{\bullet}$OH) usually considered as the primary oxidant (Herrmann et al., 2010; Smith et al., 2014). The significance of photosensitized chemistry in atmospheric aerosols has recently been reviewed (George et al., 2015). For instance, triplet excited states of organic compounds (^{3}C*) from the irradiation of light-absorbing organics such as non-phenolic aromatic carbonyls (Canonica et al., 1995; Anastasio et al., 1997; Vione et al., 2006; Smith et al., 2014) have been reported to oxidize phenols at higher rates and with greater aqSOA yields compared to $^{\bullet}$OH (Sun et al., 2010; Smith et al., 2014; Yu et al., 2014; Smith et al., 2016). Aside from being an oxidant, ^{3}C* can also be a precursor of singlet oxygen ($^1O_2$), superoxide ($O_2^{\bullet-}$) or hydroperoxyl ($^{\bullet}HO_2$) radical, and $^{\bullet}$OH (via $HO_2^{\bullet}/O_2^{\bullet-}$ formation) upon reactions with O_2 and substrates (e.g., phenols) (George et al., 2018). The ^{3}C* concentration in typical fog water has been estimated to be > 25 times than that of $^{\bullet}$OH, making ^{3}C* the primary photo-oxidant for biomass burning phenolic compounds (Kaur and Anastasio, 2018; Kaur et al., 2019). Recent works on triplet-driven oxidation of phenols have mainly focused on changes of physicochemical properties (e.g., light absorption) and aqSOA yield (e.g., Smith et al., 2014, 2015, 2016), with few reports on reaction pathways and products (e.g., Yu et al., 2014; Chen et al., 2020; Jiang et al., 2021).

Inorganic salts such as ammonium nitrate are major components of aerosols and cloud/fog water. In cloud and fog water, the concentrations of inorganic nitrate can vary from 50 μM to > 1000 μM, with higher levels typically noted under polluted conditions (Munger et al., 1983; Collett et al., 1998; Zhang and Anastasio, 2003; Li et al., 2011; Giulianelli et al., 2014; Bianco et al., 2020). Upon photolysis (Vione et al., 2006; Herrmann, 2007; Scharko et al., 2014), inorganic nitrate in cloud and fog water can contribute to BrC (Minero et al., 2007) and aqSOA formation (Huang et al., 2018; Klodt et al., 2019; Zhang et al., 2021) by generating $^{\bullet}$OH and nitrating agents (e.g., $^{\bullet}NO_2$). For example, the aqSOA yields from the photo-oxidation of phenolic carbonyls in ammonium nitrate are twice as high as that in ammonium sulfate solution (Huang et al., 2018). Nitration is a significant process in the formation of light-absorbing organics or BrC in the atmosphere (Jacobson, 1999; Kahnt et al., 2013; Mohr et al., 2013; Laskin et al., 2015; Teich et al., 2017; Li et al., 2020). Moreover, nitrate photolysis has been proposed to be a potentially important process for SO_2 oxidation and SOA formation via the generation of $^{\bullet}$OH, $^{\bullet}NO_2$, and N(III) within particles (Gen et al., 2019a, 2019b; Zhang et al., 2020, 2021), and it can also potentially change the morphology of atmospheric viscous particles (Liang et al., 2021). Furthermore, ammonium (NH_4^+) can react with carbonyls producing light-absorbing compounds and highly oxygenated oligomers, as well as catalyze different reactions (De Haan et al., 2009, 2011; Nozière et al., 2009, 2010, 2018; Shapiro et al., 2009; Yu et al., 2011; Lee et al., 2013; Powelson et al., 2014; Gen et al., 2018; Mabato et al., 2019). Therefore, ^{3}C* and inorganic nitrate can contribute to aqSOA and BrC formation.

Biomass burning (BB) is a significant atmospheric source of both phenolic and non-phenolic aromatic carbonyls (Rogge et al., 1998; Nolte et al., 2001; Schauer et al., 2001; Bond et al., 2004). Upon exposure to sunlight, aromatic carbonyls are excited to their triplet excited states, which can initiate oxidation leading to aqSOA formation (e.g., Smith et al., 2014; 2015, 2016). An example is vanillin (VL) (Henry's law constant of 4.56×10^5 M atm^{-1}; Yaws, 1994), a phenolic aromatic carbonyl that has been used as a model compound for methoxyphenols, which are abundant in BB emissions (Li et al., 2014; Pang et al., 2019a). The aqueous $^\bullet$OH oxidation and direct photodegradation of VL have been shown to yield low-volatility products, although these findings were based on 254-nm irradiation (Li et al., 2014). Photodegradation kinetics and aqSOA yields have been reported for direct VL photodegradation under simulated sunlight (Smith et al., 2016), with oxygenated aliphatic-like compounds (high H:C, ≥ 1.5 and low O:C, ≤ 0.5 ratios) noted as the most likely products (Loisel et al., 2021). Additionally, aqueous-phase reactions of phenols with reactive nitrogen species have been proposed to be a significant source of nitrophenols and SOA (Grosjean, 1985; Kitanovski et al., 2014; Kroflič et al., 2015, 2021; Pang et al., 2019a; Yang et al., 2021). For instance, nitrite-mediated VL photo-oxidation can generate nitrophenols, and the reactions are influenced by nitrite/VL molar ratios, pH, and the presence of $^\bullet$OH scavengers (Pang et al., 2019a). Nitrate and ammonium are also among the main biomass burning aerosol components (Xiao et al., 2020; Zielinski et al., 2020). As BB aerosols are typically internally mixed with other aerosol components (Zielinski et al., 2020), VL may coexist with ammonium nitrate in BB aerosols. The direct photosensitized oxidation of VL in the absence and presence of ammonium nitrate may then reveal insights into the atmospheric processing of BB aerosols. Moreover, the ^{3}C* of non-phenolic aromatic carbonyls (e.g., 3,4-dimethoxybenzaldehyde, DMB; a non-phenolic aromatic carbonyl) (Smith et al., 2014; Yu et al., 2014; Jiang et al., 2021) and phenolic aromatic carbonyls (e.g., acetosyringone, vanillin) (Smith et al., 2016) have been shown to oxidize phenols, but the reaction products from the latter are unknown.

Previous works on aqSOA formation via triplet-mediated oxidation are mostly based on reactions between phenols and a non-phenolic aromatic carbonyl as triplet precursor (e.g., Smith et al., 2014; Yu et al., 2014; Jiang et al., 2021). Also, studies examining the effects of inorganic nitrate on aqSOA formation and properties remain limited. The present study aimed to evaluate aqSOA formation via the direct photosensitized oxidation of a triplet precursor (VL) alone. Furthermore, aqSOA formation via the direct photosensitized oxidation of VL in the presence of ammonium nitrate was also examined. Accordingly, the main goals of this study are (1) to compare aqSOA formation in cloud/fog water via the direct photosensitized oxidation of VL in the absence and presence of ammonium nitrate, (2) to evaluate the influences of O_2, solution pH, and reactants concentration and molar ratios on the reactions, (3) to investigate the participation of ammonium in the direct photosensitized oxidation of VL in the presence of ammonium nitrate, and (4) to examine aqSOA formation from the oxidation of guaiacol, a non-carbonyl phenol, via photosensitized reactions of VL. To achieve these goals, solutions composed of either VL only or VL in the presence of ammonium nitrate were subjected to simulated sunlight irradiation under atmospherically relevant cloud and fog conditions. Solutions composed of VL in the presence of sodium nitrate were also examined for comparison with the presence of ammonium nitrate. The reactions were characterized based on VL decay kinetics, detected products, and light absorbance changes. Finally, we proposed aqSOA formation pathways via the direct photosensitized oxidation of VL in the

98 absence and presence of ammonium nitrate. This work presents a comprehensive comparison of aqSOA formation from the

99 direct photosensitized oxidation of VL in the absence and presence of ammonium nitrate.

100

101 **2 Methods**

102 **2.1 Aqueous-phase photo-oxidation experiments**

103 Photo-oxidation experiments were performed in a custom-built quartz photoreactor. The solutions (initial volume of 500 mL)

104 were continuously mixed throughout the experiments using a magnetic stirrer. The solutions were bubbled with synthetic air

105 or nitrogen (N_2) (> 99.995%) (0.5 dm^3/min) for 30 min before irradiation to achieve air- or N_2-saturated conditions,

106 respectively, and the bubbling was continued throughout the reactions (Du et al., 2011; Chen et al., 2020). The aim of the air-

107 saturated experiments was to enable the generation of secondary oxidants ($^1O_2$, $O_2^{\bullet-}$/$^{\bullet}HO_2$, $^{\bullet}OH$) from $^3VL^*$ as O_2 is present.

108 Conversely, the N_2-saturated experiments would inhibit the formation of these secondary oxidants, which can lead to $^3VL^*$-

109 driven reactions (Chen et al., 2020). Comparison of results of air and N_2-saturated experiments can yield information on the

110 reaction pathways that require O_2 involved in the direct photosensitized oxidation of VL. Solutions were irradiated through

111 the quartz window of the reactor using a xenon lamp (model 6258, Ozone free xenon lamp, 300 W, Newport) equipped with

112 a longpass filter (20CGA-305 nm cut-on filter, Newport) to eliminate light below 300 nm. Cooling fans positioned around the

113 photoreactor and lamp housing maintained reaction temperatures at 27 ± 2 °C. The averaged initial photon flux in the reactor

114 from 300 to 380 nm measured using a chemical actinometer (2-nitrobenzaldehyde) was 2.6×10^{15} photons cm^{-2} s^{-1} nm^{-1} (Fig.

115 S1). Although the concentration of VL in cloud/fog water has been estimated to be < 0.01 mM (Anastasio et al., 1997), a higher

116 VL concentration (0.1 mM) was used in this study to guarantee sufficient signals for product identification (Vione et al., 2019).

117 The chosen ammonium nitrate (AN) or sodium nitrate (SN) concentration (1 mM) was based on values observed in cloud and

118 fog water (Munger et al., 1983; Collett et al., 1998; Zhang and Anastasio, 2003; Li et al., 2011; Giulianelli et al., 2014; Bianco

119 et al., 2020). It should be noted that this study is not intended to identify the concentrations of ammonium nitrate that would

120 affect the kinetics but to examine the effect of ammonium nitrate on aqSOA formation from the direct photosensitized

121 oxidation of VL. Moreover, the photo-oxidation of guaiacol (GUA) (0.1 mM), a non-carbonyl phenol, in the presence of VL

122 (0.1 mM) was studied. The GUA experiments allowed us to examine aqSOA formation from the oxidation of phenols by $^3VL^*$.

123 Samples (10 mL) were collected hourly for a total of 6 h for offline chemical and optical analyses. VL (and GUA) decay

124 kinetics measurements (calibration curves for VL and GUA standard solutions; Fig. S2), product characterization, small

125 organic acids measurements, and absorbance measurements were conducted using ultra-high-performance liquid

126 chromatography with photodiode array detector (UHPLC-PDA), UHPLC coupled with quadrupole time-of-flight mass

127 spectrometry (UHPLC-qToF-MS) equipped with an electrospray ionization (ESI) source and operated in the positive ion mode

128 (the negative ion mode signals were too low for our analyses), ion chromatography (IC), and UV-Vis spectrophotometry,

129 respectively. Each experiment was repeated independently at least three times and measurements were done in triplicate. The

130 reported decay rate constants and absorbance enhancement are the average of results from triplicate experiments, and the

131   corresponding errors represent one standard deviation. The mass spectra are based on the average of results from duplicate

132   experiments. The Supporting Information (Text S1 to S6) provides details on the materials and analytical procedures. The

133   pseudo-first-order rate constant (k') for VL decay was determined using the following equation (Huang et al., 2018):

134

$$ln\left([VL]_t/[VL]_0\right) = -k't \qquad \text{(Eq. 1)}$$

136

137   where $[VL]_t$ and $[VL]_0$ are the concentrations of VL at time t and 0, respectively. Replacing VL with GUA in Eq. 1 enabled

138   the calculation of GUA decay rate constant. The decay rate constants were normalized to the photon flux measured for each

139   experiment through dividing k' by the measured 2-nitrobenzaldehyde (2NB) decay rate constant, j(2NB) (see Text S6 for more

140   details).

141   **2.2 Calculation of normalized abundance of products**

142   Comparisons of peak abundance in mass spectrometry have been used in many recent studies (e.g., Lee et al., 2014;

143   Romonosky et al., 2017; Wang et al., 2017; Fleming et al., 2018; Song et al., 2018; Klodt et al., 2019; Ning et al., 2019) to

144   show the relative importance of different types of compounds (Wang et al., 2021). However, ionization efficiency may greatly

145   vary for different classes of compounds (Kebarle, 2000; Schmidt et al., 2006; Leito et al., 2008; Perry et al., 2008; Kruve et

146   al., 2014), and so uncertainties may arise from comparisons of peak areas among compounds. In this work, we assumed equal

147   ionization efficiency of different compounds, which is commonly used to estimate O:C ratios of SOA (e.g., Bateman et al.,

148   2012; Lin et al., 2012; Laskin et al., 2014; De Haan et al., 2019), to calculate their normalized abundance. The normalized

149   abundance of a product, [P] (unitless), was calculated as follows:

$$[P] = \frac{A_{P,t}}{A_{VL,t}} \cdot \frac{[VL]_t}{[VL]_0} \qquad \text{(Eq. 2)}$$

151

152   where $A_{P,t}$ and $A_{VL,t}$ are the extracted ion chromatogram (EIC) peak areas of the product P and VL from UHPLC-qToF-MS

153   analyses at time t, respectively; $[VL]_t$ and $[VL]_0$ are the VL concentrations (μM) determined using UHPLC-PDA at time t and

154   0, respectively. Here, we relied on the direct quantification of [VL] using UHPLC-PDA (see Fig. S2 for VL calibration curve).

155   We emphasize that the normalized abundance of products in this study is a semi-quantitative analysis intended to provide an

156   overview of how the signal intensities changed under different experimental conditions but not to quantify the absolute

157   concentration of products. Also, as it is based on comparisons of peak abundance from UHPLC-qToF-MS analyses, the

158   normalized abundance of products in this study is associated with intrinsic uncertainties due to the variability in ionization

159   efficiencies for various compounds. Moreover, the major products detected in this study are probably those with high

160   concentration or high ionization efficiency in the positive ESI mode. The use of relative abundance (product peaks are

161   normalized to the highest peak) (e.g., Lee et al., 2014; Romonosky et al., 2017; Fleming et al., 2018; Klodt et al., 2019) would

162 yield the same major products reported. Typical fragmentation behavior observed in MS/MS spectra for individual functional

163 groups from Holčapek et al. (2010) are outlined in Table S1.

3 Results and Discussion

3.1 Kinetics, mass spectrometric, and absorbance changes analyses during the direct photosensitized oxidation of VL in the aqueous phase

167 For clarity purposes, the reactions involving reactive species referred to in the following discussions are provided in Table 1.

168 Table 2 summarizes the reaction conditions, initial VL (and GUA) decay rate constants, normalized abundance of products,

169 and average carbon oxidation state ($<OS_c>$) (of the 50 most abundant products). In general, the 50 most abundant products

170 contributed more than half of the total normalized abundance of products and can serve as representative products for

171 discussions of reaction pathways and calculation of the $<OS_c>$.

172 As shown in Figure S3, VL underwent oxidation both directly and in the presence of ammonium (and sodium) nitrate

173 upon simulated sunlight illumination. VL absorbs light and is promoted to its excited singlet state ($^1VL^*$), then undergoes

174 intersystem crossing (ISC) to the excited triplet state, $^3VL^*$. In principle, $^3VL^*$ can oxidize ground-state VL (Type I

175 photosensitized reactions) via H-atom abstraction/electron transfer and form $O_2^{\bullet-}$ or $HO_2^{\bullet}$ in the presence of O_2 (George et al.,

176 2018), or react with O_2 (Type II photosensitized reactions) to yield $^1O_2$ via energy transfer or $O_2^{\bullet-}$ via electron transfer (Lee et

177 al., 1987; Foote et al., 1991). The disproportionation of $HO_2^{\bullet}/O_2^{\bullet-}$ (Anastasio et al., 1997) form hydrogen peroxide (H_2O_2),

178 which is a photolytic source of $^{\bullet}OH$. Overall, air-saturated conditions, in which O_2 is present, enable the generation of

179 secondary oxidants ($^1O_2$, $O_2^{\bullet-}/^{\bullet}HO_2$, $^{\bullet}OH$) from $^3VL^*$. Moreover, $^{\bullet}OH$, $^{\bullet}NO_2$, and NO_2^-/HNO_2, i.e., N(III), generated via nitrate

180 photolysis (Reactions 1–3; Table 1), can also oxidize or nitrate VL. In this work, the direct photosensitized oxidation of VL in

181 the absence (VL only experiments) and presence of ammonium nitrate are referred to as VL* and VL+AN, respectively.

3.1.1 VL photo-oxidation under N_2 and air-saturated conditions

183 As previously stated, the N_2-saturated experiments would inhibit the formation of secondary oxidants ($^1O_2$, $O_2^{\bullet-}/^{\bullet}HO_2$, $^{\bullet}OH$)

184 from $^3VL^*$, facilitating $^3VL^*$-driven reactions (Chen et al., 2020). In contrast, the air-saturated experiments can enable the

185 generation of these secondary oxidants from $^3VL^*$ as O_2 is present. Moreover, for experiments conducted under three saturated

186 gases (air, O_2, and N_2), the rate constant for 4-ethylguaiacol (a non-carbonyl phenol) loss by $^3DMB^*$ decreased in the order of

187 air > N_2 > O_2. This was attributed to the presence of O_2, resulting in a synergistic effect of $^1O_2$ and $^3C^*$ under air-saturated

188 conditions (Chen et al., 2020). The differences in air and N_2-saturated experiments can then be used to infer the role of reaction

189 pathways that require O_2 in the direct photosensitized oxidation of VL. The photosensitized oxidation of VL under both N_2-

190 and air-saturated conditions (Fig. S3a) were carried out at pH 4, which is representative of moderately acidic aerosol and cloud

191 pH values (Pye et al., 2020). No significant VL loss was observed for dark experiments. The oxidation of ground-state VL by

192 $^3VL^*$ via H-atom abstraction or electron transfer can form phenoxy (which is in resonance with a carbon-centered

193   cyclohexadienyl radical that has a longer lifetime) and ketyl radicals (Neumann et al., 1986a, 1986b; Anastasio et al., 1997).

194   The coupling of phenoxy radicals or phenoxy and cyclohexadienyl radicals can form oligomers as observed for both N_2- and

195   air-saturated experiments (see discussions later). However, the minimal decay of VL under N_2-saturated condition indicates

196   that these radicals probably decayed via back-hydrogen transfer to regenerate VL (Lathioor et al., 1999). A possible

197   explanation for this is the involvement of O_2 in the secondary steps of VL decay. For instance, a major fate of the ketyl radical

198   is reaction with O_2 (Anastasio et al., 1997). In the absence of O_2, radical formation occurs, but the forward reaction of ketyl

199   radical and O_2 is blocked, leading to the regeneration of VL as suggested by the minimal VL decay. Aside from potential

200   inhibition of secondary oxidants generation (Chen et al., 2020), N_2 purging may have also hindered the secondary steps for

201   VL decay.

202   Contrastingly, the VL decay rate constant for VL* under air-saturated conditions was 4 times higher than under N_2-

203   saturated conditions (Table 2). As mentioned earlier, secondary oxidants ($^1O_2$, $O_2^{\bullet-}$/$^{\bullet}HO_2$, $^{\bullet}OH$) can be generated from $^3VL^*$

204   when O_2 is present (under air-saturated conditions). However, the direct photosensitized oxidation of VL in this study is likely

205   governed by $^3VL^*$ and that these secondary oxidants have only minor participation. $^1O_2$ is also a potential oxidant for phenols

206   (Herrmann et al., 2010; Minella et al., 2011; Smith et al., 2014), but $^1O_2$ reacts much faster (by ~60 times) with phenolate ions

207   than neutral phenols (Tratnyek and Hoigne, 1991; Canonica et al., 1995; McNally et al., 2005). Under the pH values (pH 2.5

208   to 4) considered in this study, the amount of phenolate ion is negligible (pK_a of VL = 7.9), so the reaction between VL and $^1O_2$

209   should be slow. Interestingly, however, both $^3C^*$ and $^1O_2$ have been shown to be important in the photo-oxidation of 4-

210   ethylguaiacol (pK_a = 10.3) by $^3DMB^*$ (solution with pH of ~3) (Chen et al., 2020). Furthermore, while the irradiation of other

211   phenolic compounds can produce H_2O_2, a precursor for $^{\bullet}OH$ (Anastasio et al., 1997), the amount of H_2O_2 is small. Based on

212   this, only trace amounts of H_2O_2 were likely generated from VL* (Li et al., 2014) under-air saturated conditions, suggesting

213   that contribution from $^{\bullet}OH$ was minor. Overall, these suggest that the direct photosensitized oxidation of VL in this study is

214   mainly driven by $^3VL^*$.

215   The VL decay rate constant for VL+AN under air-saturated conditions was also higher (6.6 times) than under N_2-

216   saturated conditions, possibly due to reactions facilitated by nitrate photolysis products that may have been enhanced in the

217   presence of O_2 (Vione et al., 2005; Kim et al., 2014; Pang et al., 2019a). As shown later, more N-containing species were

218   observed for VL+AN under air-saturated conditions than under N_2-saturated conditions. An example is enhanced VL nitration

219   likely from increased $^{\bullet}NO_2$ formation such as from the reaction of $^{\bullet}OH$ and $O_2^{\bullet-}$ with NO_2^- (Reactions 4 and 5, respectively;

220   Table 1) or the autoxidation of $^{\bullet}NO$ from NO_2^- photolysis (Reactions 6–9; Table 1) in aqueous solutions (Pang et al., 2019a).

221   Nevertheless, the comparable decay rate constants for VL* and VL+AN imply that $^3VL^*$ chemistry still dominates even at

222   1:10 molar ratio of VL/AN. This can be attributed to the much higher molar absorptivity of VL compared to that of nitrate

223   (Fig. S1) and the high VL concentration (0.1 mM) used in this study. The quantification of the oxidants in our reaction systems

224   is not explored here and require additional work. In essence, the N_2-saturated experiments suggest that the secondary steps for

225 VL decay via ^{3}VL* may require to O_2 proceed. Nonetheless, further study on the impact of O_2 on the reactive intermediates

226 involved is required to understand the exact mechanisms occurring under air-saturated conditions.

227   The products from VL* under N_2-saturated conditions were mainly oligomers (e.g., $C_{16}H_{14}O_4$) (Fig. 1a), consistent

228 with triplet-mediated oxidation forming higher molecular weight products, with less fragmentation relative to oxidation by

229 $^•$OH (Yu et al., 2014; Chen et al., 2020). A threefold increase in the normalized abundance of products was noted upon addition

230 of AN (VL+AN under N_2-saturated conditions; Fig. 1b), and in addition to oligomers, functionalized monomers (e.g., $C_8H_6O_5$)

231 and N-containing compounds (e.g., $C_8H_9NO_3$; No. 3, Table S2) were also observed, in agreement with $^•$OH-initiated oxidation

232 yielding more functionalized/oxygenated products compared to triplet-mediated oxidation (Yu et al., 2014; Chen et al., 2020).

233 Oligomers, functionalized monomers (e.g., demethylated VL; Fig. S4), and N-containing compounds (e.g., $C_{16}H_{10}N_2O_9$; No.

234 4, Table S2) (for VL+AN) had higher normalized abundance under air-saturated conditions (Figs. 1c-d), attributable to efficient

235 ^{3}VL*-initiated oxidation and enhanced VL nitration in the presence of O_2. For both VL* and VL+AN under air-saturated

236 conditions, the most abundant product was $C_{10}H_{10}O_5$ (No. 5, Table S2), a substituted VL. Irradiation of VL by 254-nm lamp

237 has also been reported to lead to VL dimerization and functionalization via ring-retaining pathways, as well as small oxygenates

238 formation but only when $^•$OH from H_2O_2 were involved (Li et al., 2014). In this work, small organic acids (e.g., formic acid)

239 were observed from both VL* and VL+AN under air-saturated conditions (Fig. S5) due to simulated sunlight that could access

240 the 308-nm VL band (Smith et al., 2016). Interestingly, we observed a potential imidazole derivative ($C_5H_5N_3O_2$; No. 6, Table

241 S2) from VL+AN under air-saturated conditions (Fig. 1d), which may have formed from reactions induced by ammonium.

242 This compound was not observed in a parallel experiment in which AN was replaced with SN (Fig. S6a; see Sect. 3.1.3 for

243 discussion).

244   The potential aqSOA formation pathways via the direct photosensitized oxidation of VL in the absence and presence

245 of AN in this study are summarized in Fig. 2. At pH 4, ^{3}VL*-initiated reactions yielded oligomeric species such as $C_{16}H_{12}O_6$

246 and $C_{22}H_{22}O_6$. Earlier works on phenolic aqSOA formation have reported that oligomers can form via the coupling of phenoxy

247 radicals or phenoxy and cyclohexadienyl radicals (Sun et al., 2010; Yu et al., 2014; Vione et al., 2019). In this work, phenoxy

248 radicals (in resonance with a carbon-centered cyclohexadienyl radical) can be generated from several processes such as the

249 oxidation of ground-state VL by ^{3}VL* via H-atom abstraction or electron transfer coupled with proton transfer from the

250 phenoxyl radical cation or from solvent water (Neumann et al., 1986a, 1986b; Anastasio et al., 1997) and photoinduced O-H

251 bond-breaking (Berto et al., 2016). Also, similar reactions can be initiated by $^•$OH (Gelencsér et al., 2003; Hoffer et al., 2004;

252 Chang and Thompson, 2010; Sun et al., 2010), which in this study can be generated from the reaction between ^{3}VL* and O_2,

253 as well as nitrate photolysis. Trace amounts of H_2O_2 could be formed during VL photodegradation (Li et al., 2014), similar to

254 the case of other phenolic compounds (Anastasio et al., 1997). In addition, ring-opening products (Fig. S5) from fragmentation

255 in both VL* and VL+AN may have reacted with VL or dissolved ammonia to generate $C_{10}H_{10}O_5$ (No. 5, Table S2) (Pang et

256 al., 2019b) or a potential imidazole derivative ($C_5H_5N_3O_2$; No. 6, Table S2), respectively. Moreover, nitrate photolysis products

257 promoted functionalization and nitration (e.g., $C_{16}H_{10}N_2O_9$; No. 4, Table S2).

The molecular transformation of VL upon photosensitized oxidation was examined using the van Krevelen diagrams (Fig. S7). For all experiments (A1-14; Table 2) in this study, the O:C and H:C ratios of the products were similar to those observed from the aging of other phenolic compounds (Yu et al., 2014) and BB aerosols (Qi et al., 2019). Under N_2-saturated conditions, oligomers with O:C ratios ≤ 0.6 were dominant in VL*, while smaller molecules ($n_c \leq 8$) with higher O:C ratios (up to 0.8) were also observed for VL+AN. In contrast, more products with higher O:C ratios (≥ 0.6) were noted under air-saturated conditions for both VL* and VL+AN. For experiments A5 to A8, H:C ratios were mostly around 1.0 and double bond equivalent (DBE) values were typically (58% of the 50 most abundant products) > 7, indicating that the products were mainly oxidized aromatic compounds (Xie et al., 2020). Compounds with H:C ≤ 1.0 and O:C ≤ 0.5 are common for aromatic species, while compounds with H:C ≥ 1.5 and O:C ≤ 0.5 are typical for more aliphatic species (Mazzoleni et al., 2012; Kourtchev et al., 2014; Jiang et al., 2021). In contrast, Loisel et al. (2021) reported mainly oxygenated aliphatic-like compounds from the direct irradiation of VL (0.1 mM), attributable to their use of ESI in the negative ion mode, which has higher sensitivity for detecting compounds such as carboxylic acids (Holčapek et al., 2010; Liigand et al., 2017), and solid-phase extraction (SPE) procedure causing the loss of some oligomers (LeClair et al., 2012; Zhao et al., 2013; Bianco et al., 2019). Among experiments A5 to A8, VL+AN under air-saturated conditions (A7) had the highest normalized abundance of products and $<OS_c>$, probably due to the combined influence of ^{3}VL* and enhanced VL nitration in the presence of O_2. Our measured $<OS_c>$ for all experiments range from -0.28 to +0.12, while other studies on phenolic aqSOA formation reported $<OS_c>$ ranging from -0.14 to +0.47 (Sun et al., 2010) and 0.04 to 0.74 (Yu et al., 2014). The $<OS_c>$ in this study likely were lower estimates since we excluded contributions from ring-opening products, which may have higher OS_c values as these products are not detectable in the positive ion mode. In brief, more oxidized aqSOA and higher normalized abundance of products such as oligomers and functionalized monomers were noted under air-saturated conditions due to efficient VL oxidation by ^{3}VL* in the presence of O_2. Compared to N_2-saturated condition, the higher normalized abundance of N-containing products under air-saturated condition for VL+AN (at pH 4) suggests a potential enhancement of VL nitration in the presence of O_2.

Illumination of phenolic aromatic carbonyls with high molar absorptivities ($\varepsilon_{\lambda max}$) (~8 to 22×10^3 M^{-1} cm^{-1}) leads to an overall loss of light absorption but increased absorbance at longer wavelengths (> 350 nm), where the carbonyls did not initially absorb light (Smith et al., 2016). Fig. 3a illustrates the changes in total absorbance from 350 to 550 nm of VL* and VL+AN under N_2- and air-saturated conditions. The absorption spectra of VL* under air- and N_2- saturated conditions (pH 4) at different time intervals are shown in Fig. S8. For both VL* and VL+AN, evident absorbance enhancement was observed under air-saturated conditions, while the absorbance changes under N_2-saturated conditions were minimal, consistent with the VL decay trends. Dimers and functionalized products have been shown to contribute to chromophore formation for the aqueous photo-oxidation of guaiacyl acetone (another aromatic phenolic carbonyl) by ^{3}DMB* (Jiang et al., 2021). Based on this, the higher normalized abundance of oligomers, which have large, conjugated π-electron systems (Chang and Thompson, 2010), and hydroxylated products (Li et al., 2014; Zhao et al., 2015) observed under air-saturated conditions have contributed to the absorbance enhancement. However, it is worth noting that the products detected may not have contributed significantly to the total products formed and hence may not be the primary contributors to the absorbance enhancement. As mentioned earlier,

292 the major products detected in this study are probably those with high concentration or high ionization efficiency in the positive
293 ESI mode. In other words, the absorbance enhancement may not necessarily correlate directly with the products detected.

294   Correlating speciated chromophores with absorbance changes may be useful in demonstrating how aqSOA influence
295 the Earth's radiative balance and identifying chemical reactions that can affect the overall light absorption by aqSOA. This
296 can be accomplished by using liquid chromatography coupled with photodiode array (PDA) detector and high-resolution mass
297 spectrometry (LC/PDA/HRMS platform) (e.g., Lin et al., 2017; Jiang et al., 2021; Misovich et al., 2021). In our experiments,
298 VL (and GUA) concentration measurements, product characterization, and absorbance measurements were performed using
299 UHPLC-PDA, UHPLC-qToF-MS, and UV-Vis spectrophotometry, respectively. A similar approach is then possible using the
300 current methods in this work by matching the retention time (RT) of the products detected using UHPLC-ToF-MS with that
301 in the PDA. However, the concentration of the chromophores in this study is below the detection limit of the PDA based on
302 the lack of distinct PDA signals from the products. Absorbance increase at > 350 nm has also been reported for the
303 photosensitized oxidation of phenol and 4-phenoxyphenol (De Laurentiis et al., 2013a, 2013b) and direct photolysis of tyrosine
304 and 4-phenoxyphenol (Bianco et al., 2014) in which dimers have been identified as initial substrates. The continuous
305 absorbance enhancement throughout 6 h of irradiation correlated with the observation of oligomers and nitrated compounds
306 after irradiation. However, the increasing concentration of small organic acids (Fig. S5) throughout the experiments suggests
307 that fragmentation, which results in the decomposition of initially formed oligomers and formation of smaller oxygenated
308 products (Huang et al., 2018), is important at longer irradiation times. Overall, these trends establish that compared to N_2-
309 saturated conditions, VL oxidation by $^3VL^*$ under air-saturated conditions (O_2 is present) enabled the efficient formation of
310 light-absorbing compounds from both VL* and VL+AN.

311 **3.1.2 VL photo-oxidation under varying pH conditions**

312 The reactions of $^3C^*$ (Smith et al., 2014, 2015, 2016), aromatic photonitration by nitrate (Machado and Boule, 1995; Dzengel
313 et al., 1999; Vione et al., 2005; Minero et al., 2007), and N(III)-mediated VL photo-oxidation (Pang et al., 2019a) have been
314 demonstrated to be pH-dependent. In this study, the effect of pH on the direct photosensitized oxidation of VL was investigated
315 over the pH range of 2.5 to 4, which is within typical cloud pH values (2-7) (Pye et al., 2020). The decay rate constants for
316 both VL* and VL+AN increased by 1.6 and 1.4 times, respectively, as pH decreased from 4 to 2.5 (Table 2). These differences
317 in decay rate constants are small but statistically significant ($p < 0.05$). The pK_a for the $^3VL^*$ has been reported to be 4.0 (Smith
318 et al., 2016). As there is a greater fraction of $^3VL^*$ that are protonated at pH 2.5 (0.96) than at pH 4 (0.50), it is possible that
319 the pH dependence of the VL decay rate constants observed in this study is due to $^3VL^*$ being more reactive in its protonated
320 form. Smith et al. (2016) also observed a pH dependence for the direct photodegradation of VL (0.005 mM) (rate constants at
321 pH ≤ 3 are ~two times lower than at pH ≥ 5) which has been attributed to the sensitivity of the excimer of VL (i.e., the charge-
322 transfer complex formed between an excited state VL molecule and a separate ground state VL molecule; Birks, 1973, Turro
323 et al., 2010) to acid-base chemistry. The opposite trend observed in this study for 0.1 mM VL may be due to the reactivities of
324 the protonated and neutral forms of $^3VL^*$ being dependent on VL concentration (Smith et al., 2016). The quantum yield for

direct VL photodegradation is higher at pH 5 than at pH 2 for 0.005 mM VL, but they are not statistically different for 0.03 mM VL (Smith et al., 2016). As pH decreases, the higher reactivity of ^{3}VL* and sensitivity of the excimer of VL to acid-base chemistry may have led to faster VL photo-oxidation. Similar to pH 4 experiments, comparable decay rate constants between VL* and VL+AN were also noted at pH < 4, again suggesting the predominant role of ^{3}VL* chemistry compared to nitrate, likely due to the high VL concentration (0.1 mM) used in this study.

      As pH decreased, the normalized abundance of products, particularly oligomers and functionalized monomers, was higher for both VL* and VL+AN, consistent with ^{3}VL* potentially being more reactive in its protonated form. The most abundant products observed were a substituted VL ($C_{10}H_{10}O_5$; No. 5, Table S2) and VL dimer ($C_{16}H_{14}O_6$; No. 7, Table S2) at pH 4 and pH < 4, respectively (Figs. 1c-h). Furthermore, a tetramer ($C_{31}H_{24}O_{11}$) was observed only in VL* at pH 2.5. For VL+AN, the normalized abundance of N-containing compounds was also higher at lower pH (Table 2), likely due to increased $^{\bullet}$OH and $^{\bullet}$NO$_2$ formation, which may be caused by the dependence of N(III) (NO$_2^-$ + HONO) speciation on solution acidity (Pang et al., 2019a). At pH 3.3, half of N(III) exists as HONO (Fischer and Warneck, 1996; Pang et al., 2019a), which has a higher quantum yield for $^{\bullet}$OH formation than that of NO$_2^-$ in the near-UV region (Arakaki et al., 1999; Kim et al., 2014). Also, NO$_2^-$/HONO can generate $^{\bullet}$NO$_2$ via oxidation by $^{\bullet}$OH (Reactions 4 and 10; Table 1) (Pang et al., 2019a). At pH < 4, ^{3}VL* likely have higher reactivity as suggested by the increased normalized abundance of oligomers (e.g., $C_{16}H_{14}O_6$; No. 7, Table S2 and $C_{31}H_{24}O_{11}$) and N-containing compounds (e.g., $C_{16}H_{10}N_2O_9$; No. 4, Table S2 and $C_{13}H_{14}N_2O_{10}$) (Fig. 2). The most abundant product at pH < 4, $C_{16}H_{14}O_6$ (No. 7, Table S2), is likely a C−O coupled dimer. In previous studies on phenolic aqSOA formation, the generation of phenolic dimers has been proposed to occur via C−C or C−O coupling of phenoxy radicals (Sun et al., 2010; Yu et al., 2014; Huang et al., 2018; Chen et al., 2020; Misovich et al., 2021). Similarly, functionalized monomers such as $C_7H_6O_3$ (demethylated VL; No. 8, Table S2) and hydroxylated products (e.g., $C_8H_8O_4$; No. 9, Table S2) also had increased normalized abundance for both VL* and VL+AN. The formation of $C_7H_6O_3$ (No. 8, Table S2), which varies from the structure of VL by CH$_2$, can be explained by $^{\bullet}$OH addition at the carbon containing the methoxy group, succeeded by the elimination of a methoxy radical ($^{\bullet}$OCH$_3$) (Yee et al., 2013). This reaction has also been postulated for the $^{\bullet}$OH oxidation of syringol (2,6-dimethoxyphenol) (Yee et al., 2013) and transformation of DMB in a system composed of guaiacyl acetone and ^{3}DMB* (Misovich et al., 2021). The potential imidazole derivative ($C_5H_5N_3O_2$; No. 6, Table S2) was observed only at pH 4, following the pH dependence of ammonium speciation (pK_a = 9.25). Imidazole formation requires the nucleophilic attack of ammonia on the carbonyl group (Yu et al., 2011), and at pH 4, the concentration of dissolved ammonia in VL+AN was about 10 or 30 times higher than that at pH 3 or pH 2.5, respectively. For the pH values considered in this study, the O:C and H:C ratios in VL* and VL+AN had no significant differences (Figs. S7c–d and S9), but molecules with higher O:C ratios (> 0.6) were more abundant at pH < 4. In addition, the <OS$_c$> at pH < 4 for both VL* and VL+AN were higher than that at pH 4, consistent with higher <OS$_c$> observed at pH 5 compared to pH 7 for the $^{\bullet}$OH-mediated photo-oxidation of syringol (Sun et al., 2010). Essentially, the higher reactivity of ^{3}VL* and predominance of HONO over nitrite at lower pH may have resulted in higher normalized abundance of products mainly composed of oligomers and functionalized monomers.

358   Higher absorbance enhancement for both VL* and VL+AN (Fig. 3b) was observed as pH increased. To determine

359   whether the pH dependence is due to the acid-base chemistry of the products or of the reactions, the changes in the UV-Vis

360   absorption spectra of the aqSOA formed from VL* at pH 4 and 2.5 were measured over a range of pH conditions from 1.5 to

361   10.5 (Fig. S10). For both cases, the intensity of absorption at longer wavelengths significantly increased as the pH of the

362   solutions was raised. Moreover, the changes in the UV-Vis absorption spectra for the two solutions of varying pH are

363   comparable, suggesting that the observed pH dependence is rooted in acid-base chemistry of the reactions involving ^{3}VL* or

364   the excimer of VL (Smith et al., 2016), as discussed earlier.

3.1.3 Participation of ammonium in the direct photosensitized oxidation of VL in the presence of AN

366   Ammonium salts are an important constituent of atmospheric aerosols particles (Jimenez et al., 2009), and reactions between

367   dicarbonyls (e.g., glyoxal) and ammonia or primary amines form BrC (De Haan et al., 2009, 2011; Nozière et al., 2009; Shapiro

368   et al., 2009; Lee et al., 2013; Powelson et al., 2014; Gen et al., 2018; Mabato et al., 2019). Imidazole and imidazole derivatives

369   are the major products of glyoxal and ammonium sulfate reactions at pH 4 (Galloway et al., 2009; Yu et al., 2011; Sedehi et

370   al., 2013; Gen et al., 2018; Mabato et al., 2019). Here, we compared VL+AN and VL+SN at pH 4 under air-saturated conditions

371   to confirm the participation of ammonium in the photosensitized oxidation of VL. The presence of ammonium did not appear

372   to influence the kinetics of VL decay and light absorbance changes based on VL+AN and VL+SN having no statistically

373   significant difference ($p > 0.05$) with respect to VL decay rate constants (Table 2) and yielding comparable absorbance

374   enhancement (Fig. 3a), respectively. However, it is important to note that this may not be the case for lower concentrations of

375   VL. As previously stated, the reactions in this study were dominated by ^{3}VL* chemistry, likely due to the higher molar

376   absorptivity of VL than that of nitrate and the high VL concentration used. Similarly, the normalized abundance of products

377   was comparable in both experiments (A7 and A9; Table 2) with $C_{10}H_{10}O_5$ (No. 5, Table S2) as the most abundant product

378   (Figs. 1d and S6a), but in VL+SN, there was a significant amount of a VL dimer ($C_{15}H_{12}O_8$; No. 10, Table S2). The normalized

379   abundance of N-containing compounds was also similar for VL+AN and VL+SN but the detected N-containing compounds

380   were distinct. Aside from the potential imidazole derivative ($C_5H_5N_3O_2$; No. 6, Table S2), $C_8H_9NO_3$ (No. 3, Table S2), possibly

381   an aminophenol, was also observed from VL+AN but only under N_2-saturated conditions (Fig. 1b), probably due to further

382   oxidation by ^{3}VL*. Relative to VL+AN, the products from VL+SN had higher O:C ratios (e.g., $C_7H_4N_2O_7$; No. 11, Table S2),

383   OS_c, and $<OS_c>$ values (Table 2). In summary, while the VL decay kinetics and absorbance enhancement for VL+AN and

384   VL+SN were similar, the product analysis supports the participation of ammonium in the aqueous-phase reactions.

3.1.4 Distribution of potential BrC compounds

386   Figure S11 plots the DBE values vs. number of carbons (n_c) (Lin et al., 2018) for the 50 most abundant products from pH 4

387   experiments under air-saturated conditions, along with reference to DBE values corresponding to fullerene-like hydrocarbons

388   (Lobodin et al., 2012), cata-condensed polycyclic aromatic hydrocarbons (PAHs) (Siegmann and Sattler, 2000), and linear

389   conjugated polyenes with a general formula C_xH_{x+2}. As light absorption by BrC requires uninterrupted conjugation across a

significant part of the molecular structure, compounds with DBE/n_C ratios (shaded area in Fig. S11) greater than that of linear conjugated polyenes are potential BrC compounds (Lin et al., 2018). Based on this criterion and the observed absorbance enhancement at > 350 nm (Fig. 3), the majority of the 50 most abundant products from pH 4 experiments under air-saturated conditions were potential BrC chromophores composed of monomers and oligomers up to tetramers. However, as ESI-detected compounds in BB organic aerosols has been reported to be mainly molecules with $n_c < 25$ (Lin et al., 2018), there may be higher oligomers that were not detected in our reaction systems.

3.2 Effect of reactants concentration and molar ratios on the direct photosensitized oxidation of VL in the aqueous phase

To examine the influence of VL and AN concentration and their molar ratios on the direct photosensitized oxidation of VL, we also characterized the reaction products from lower [VL] (0.01 mM VL*; A10; Table 2), lower [VL] and equal molar ratio of VL/AN (0.01 mM VL + 0.01 mM AN; A11; Table 2), and lower [VL] and 1:100 molar ratio of VL/AN (0.01 mM VL + 1 mM AN; A12; Table 2) at pH 4. The normalized abundance of products from low [VL] experiments (A10-A12; Table 2) were up to 1.4 times higher than that of high [VL] experiments (A5 and A7; Table 2). Nevertheless, the major products for both low and high [VL] experiments were functionalized monomers (Figs. 1c-d and S12a–c) such as $C_8H_6O_4$ (No. 12, Table S2) and $C_{10}H_{10}O_5$ (No. 5, Table S2). For both VL* and VL+AN, the contribution of < 200 m/z to the normalized abundance of products was higher at low [VL] than at high [VL], while the opposite was observed for > 300 m/z (Fig. S12d). This indicates that functionalization was favored at low [VL], as supported by the higher $<OS_c>$, while oligomerization was the dominant pathway at high [VL], consistent with more oligomers or polymeric products reported from high phenols concentration (e.g., 0.1 to 3 mM) (Li et al., 2014; Slikboer et al., 2015; Ye et al., 2019). As the formation mechanism of dimers and higher oligomers during aqueous-phase reactions of phenolic compounds involves the coupling of phenoxy radicals (Kobayashi and Higashimura, 2003; Sun et al., 2010), the enhanced oligomerization at high [VL] can be attributed to an increased concentration of phenoxy radicals (in resonance with a carbon-centered cyclohexadienyl radical) at high [VL], promoting radical-radical polymerization (Sun et al., 2010; Li et al., 2014). At low [VL], the contribution of < 200 m/z to the normalized abundance of products was higher for 1:1 than 1:100 VL/AN molar ratio, suggesting the prevalence of functionalization for the former. In addition, 1:1 VL/AN (A11; Table 2) had higher $<OS_c>$ than 1:100 VL/AN (A12; Table 2), indicating the formation of more oxidized products, but had fewer N-containing compounds compared to the latter. A possible explanation is that at 1:1 VL/AN, VL may compete with NO_2^- for $\cdot OH$ (from nitrate or nitrite photolysis, Reaction 4; Table 1) and indirectly reduce $\cdot NO_2$. Similarly, hydroxylation has been suggested to be a more important pathway for 1:1 VL/nitrite than in 1:10 VL/nitrite (Pang et al., 2019a). Fragmentation, which leads to the decomposition of previously formed oligomers and generation of small, oxygenated products such as organic acids (Huang et al., 2018), may also occur for the low [VL] experiments. However, its importance would likely be observed at longer irradiation times, similar to the high [VL] experiments.

3.3 Oxidation of guaiacol by photosensitized reactions of VL

The oxidation of phenols by $^3C^*$ has been mainly studied using non-phenolic aromatic carbonyls (Anastasio et al., 1997; Smith et al., 2014, 2015; Yu et al., 2014; Chen et al., 2020) and aromatic ketones (Canonica et al., 2000) as triplet precursors. Recently, $^3VL^*$ has been shown to oxidize syringol (Smith et al., 2016), a non-carbonyl phenol, although the reaction products remain unknown. In this section, we discussed the photo-oxidation of guaiacol (GUA), a non-carbonyl phenol that is also a lignocellulosic BB pollutant (Kroflič et al., 2015), in the presence of VL (GUA+VL). The dark experiments did not show any substantial loss of VL or GUA (Fig. S3c). Due to its poor light absorption in the solar range, GUA is not an effective photosensitizer (Smith et al., 2014; Yu et al., 2014). Accordingly, direct GUA photodegradation resulted in minimal decay, which plateaued after ~3 hours. In the presence of VL, the GUA decay rate constant was 2.2 times higher due to the oxidation of GUA by $^3VL^*$. The decay rate constant of VL in GUA+VL (A14; Table 2) was 3 times slower than that of VL* (A5; Table 2), which may be due to competition between ground-state VL and GUA for reactions with $^3VL^*$ or increased conversion of $^3VL^*$ back to the ground state through the oxidation of GUA (Anastasio et al., 1997; Smith et al., 2014).

For GUA experiments, the normalized abundance of products was calculated only for GUA+VL (2.2; Table 2) as the GUA signal from the UHPLC-qToF-MS in the positive ion mode was weak, which may introduce large uncertainties during normalization. Nonetheless, the number of products detected from these experiments (178 and 844 for direct GUA photodegradation and GUA+VL, respectively) corroborates the kinetics results. The major products (Fig. 4a) from direct GUA photodegradation were $C_{14}H_{14}O_4$ (No. 13, Table S2), a typical GUA dimer, and $C_{21}H_{20}O_6$ (No. 14, Table S2), a trimer which likely originated from photoinduced O-H bond-breaking (Berto et al., 2016). In general, higher absolute signal intensities were noted for oligomers (e.g., $C_{14}H_{14}O_4$, No. 13 and $C_{21}H_{20}O_6$, No. 14, Table S2) and hydroxylated products (e.g., $C_7H_8O_4$) in GUA+VL, similar to those observed from GUA oxidation by $^3DMB^*$ or $^{\bullet}OH$ (from H_2O_2 photolysis) (Yu et al., 2014; Jiang et al., 2021). Also, a potential GUA tetramer ($C_{28}H_{26}O_8$, No. 15, Table S2) was observed only in GUA+VL, consistent with more efficient oligomer formation from the triplet-mediated oxidation of phenols relative to direct photodegradation (Yu et al., 2014). The products from the direct GUA photodegradation and GUA+VL had mostly similar OS_c values (-0.5 to 0.5) (Figs. 4b–c), falling into the criterion of biomass burning organic aerosol (BBOA) and semivolatile oxygenated organic aerosol (SV-OOA) (Kroll et al., 2011). The corresponding absorbance changes for the GUA experiments (Fig. 3c) were consistent with the observed VL and GUA decay trends and detected products. While minimal absorbance changes, which also plateaued after ~3 hours, were observed for direct GUA photodegradation, significant and continuous absorbance enhancement was noted for GUA+VL. Compared to direct GUA photodegradation, GUA oxidation by photosensitized reactions of VL occurred rapidly and yielded higher absolute signal intensities for oligomers and hydroxylated products, which likely contributed to the pronounced absorbance enhancement. These findings indicate that phenol oxidation by $^3VL^*$ can also contribute to aqSOA formation.

4 Conclusions and atmospheric implications

In this study, the direct photosensitized oxidation of VL in the absence and presence of AN under atmospherically relevant cloud and fog conditions have been shown to generate aqSOA composed of oligomers, functionalized monomers, oxygenated ring-opening products, and nitrated compounds (from VL+AN). The oligomers from these reaction systems may be rather recalcitrant to fragmentation based on their high normalized abundance, even at the longest irradiation time used in this study. Nonetheless, the increasing concentration of small organic acids over time implies that fragmentation becomes important at extended irradiation times. The reactions were observed to be influenced by O_2, pH, and reactants concentration and molar ratios. Our results suggest that O_2 could be required for the secondary steps in VL decay (e.g., the reaction of ketyl radical and O_2) via $^3VL^*$ to proceed. Compared to N_2-saturated conditions, $^3VL^*$-initiated reactions under air-saturated conditions (O_2 is present) proceeded rapidly, promoted the formation of more oxidized aqSOA, and generated products (e.g., oligomers, functionalized monomers, and N-containing compounds) with higher normalized abundance which exhibited stronger light absorption. For pH 4 experiments, the presence of both O_2 and nitrate resulted in the highest normalized abundance of products (including N-containing compounds) and $<OS_c>$, which is attributed to O_2 promoting VL nitration. Nevertheless, further work on the effect of O_2 on the reactive intermediates involved in the reactions is necessary to elucidate the mechanisms of direct photosensitized oxidation of VL under air-saturated conditions. Additionally, the formation of oligomers from the direct photosensitized oxidation of VL was promoted at low pH (< 4). Low VL concentration favored functionalization, while oligomerization prevailed at high VL concentration, consistent with past works (Li et al., 2014; Slikboer et al., 2015; Ye et al., 2019). Hydroxylation was observed to be important at equal molar ratios of VL and nitrate, likely due to VL competing with nitrite for $\cdot OH$. Furthermore, the oxidation of guaiacol, a non-carbonyl phenol, via VL photosensitized reactions was shown to form oligomers and hydroxylated products. Aromatic carbonyls and nitrophenols have been reported to be the most significant classes of BrC in cloud water heavily affected by biomass burning in the North China Plain (Desyaterik et al., 2013). Correspondingly, the most abundant products from our reaction systems (pH 4, air-saturated solutions) are mainly potential BrC chromophores. These suggest that aqSOA generated in cloud/fog water from the oxidation of biomass burning aerosols via direct photosensitized reactions and nitrate photolysis products can impact aerosol optical properties and radiative forcing, particularly for areas where biomass burning is intensive.

Ammonium (and sodium) nitrate was not found to substantially affect the VL decay rate constants, likely due to the much higher molar absorptivity of VL than nitrate and high VL concentration used in this work. However, the presence of ammonium (and sodium) nitrate promoted functionalization and nitration, indicating the significance of nitrate photolysis for aqSOA formation from biomass burning-derived compounds. This work demonstrates that nitration, which is an important process for producing light-absorbing organics or BrC (Jacobson, 1999; Kahnt et al., 2013; Mohr et al., 2013; Laskin et al., 2015; Teich et al., 2017; Li et al., 2020), can also affect the aqueous-phase processing of triplet-generating aromatics. In addition, a potential imidazole derivative observed from VL+AN at pH 4 reveals that ammonium participates in aqSOA formation from the photo-oxidation of phenolic aromatic carbonyls. This observation also suggests that the photosensitized oxidation of phenolic aromatic carbonyls in the presence of AN could be a source of imidazoles in the aqueous phase. It is

important to understand the source of imidazoles due to their possible effects on human health, their photosensitizing potential, and their effect on aerosol optical properties as BrC compounds (Teich et al., 2016).

A recent work (Ma et al., 2021) mimicking phenol oxidation by ^{3}DMB* (a non-phenolic aromatic carbonyl) in more concentrated conditions of aerosol particles containing high AN concentration (0.5 M) increased the photodegradation rate constant for guaiacyl acetone (an aromatic phenolic carbonyl with high Henry's law constant, 1.2×10^6 M atm^{-1}; McFall et al., 2020) by > 20 times which was ascribed to $^•$OH formation from nitrate photolysis (Brezonik and Fulkerson-Brekken, 1998; Chu and Anastasio, 2003). The same study also estimated that reactions of phenols with high Henry's law constants (10^6 to 10^9 M atm^{-1}) can be important for SOA formation in aerosol particles, with mechanisms mainly governed by ^{3}C* and ^{1}O$_2$ (Ma et al., 2021). Likewise, Zhou et al. (2019) reported that the direct photodegradation of acetosyringone was faster by about 6 times in the presence of 2 M NaClO$_4$. However, the opposite was noted for the photodegradation of VL in sodium sulfate or sodium nitrate, which would occur slower (~2 times slower in 0.5 M sodium sulfate and ~10 times slower in 0.124 M sodium nitrate) in aerosol particles relative to dilute aqueous phase in clouds (Loisel et al., 2021), implying that the nature of inorganic ions may have an essential role in the photodegradation of organic compounds in the aqueous phase.

The concentrations of VL and nitrate can be significantly higher in aqueous aerosol particles than what we have used to mimic cloud/fog water. As a major component of aerosols, nitrate can have concentrations as high as sulfate (Huang et al., 2014). More studies should then explore the direct photosensitized oxidation of other biomass burning-derived phenolic aromatic carbonyls, particularly those with high molar absorption coefficients. Based on our findings, the presence of nitrate should be considered for examining aqSOA formation from these reactions. The influences of reaction conditions should also be investigated to better understand the oxidation pathways. As aerosols comprise more complex mixtures of organic and inorganic compounds, it is worthwhile to explore the impacts of other potential aerosol constituents on aqSOA formation and photo-oxidation studies. This can also be beneficial in understanding the interplay among different reactions during photo-oxidation. Considering that biomass burning emissions are expected to increase continuously, further studies on these aqSOA formation pathways are strongly suggested.

Data availability.

The data used in this publication are available to the community and can be accessed by request to the corresponding author.

Author contributions.

BRGM designed and conducted the experiments; YL provided assistance in measurements and helped to analyze experimental data; YJ provided assistance in measurements; BRGM, YL, and CKC wrote the paper. All co-authors contributed to the discussion of the manuscript.

Competing interests.

The authors declare that they have no conflict of interest.

Acknowledgments.

This work was financially supported by the National Natural Science Foundation of China (41875142 and 42075100). Y.J.L acknowledges support from the Science and Technology Development Fund, Macau SAR (File no. 0019/2020/A1), the Multi-Year Research grant (No. MYRG2018-00006-FST) from the University of Macau. D.D.H. acknowledges support from the National Natural Science Foundation of China (21806108). X.L. acknowledges support from the Local Innovative and Research Teams Project of Guangdong Pearl River Talents Program (2019BT02Z546). T.N. acknowledges support from the Hong Kong Research Grants Council (21304919) and City University of Hong Kong (9610409). C.H.L. acknowledges support from the City University of Hong Kong (9610458 and 7005576).

References

Anastasio, C., Faust, B. C., and Rao, C. J.: Aromatic carbonyl compounds as aqueous-phase photochemical sources of hydrogen peroxide in acidic sulfate aerosols, fogs, and clouds. 1. Non-phenolic methoxybenzaldehydes and methoxyacetophenones with reductants (phenols), Environ. Sci. Technol., 31, 218−232, https://doi.org/10.1021/es960359g, 1997.

Arakaki, T., Miyake, T., Hirakawa, T., and Sakugawa, H.: pH dependent photoformation of hydroxyl radical and absorbance of aqueous-phase N(III) (HNO_2 and NO_2^-), Environ. Sci. Technol., 33, 2561−2565, https://doi.org/10.1021/es980762i, 1999.

Bateman, A. P., Laskin, J., Laskin, A., and Nizkorodov, S. A.: Applications of high-resolution electrospray ionization mass spectrometry to measurements of average oxygen to carbon ratios in secondary organic aerosols, Environ. Sci. Technol., 46, 8315–8324, https://doi.org/10.1021/es3017254, 2012.

Benedict, K. B., McFall, A. S., and Anastasio, C.: Quantum yield of nitrite from the photolysis of aqueous nitrate above 300 nm, Environ. Sci. Technol., 51, 4387−4395, https://doi.org/10.1021/acs.est.6b06370, 2017.

Berto, S., De Laurentiis, E., Tota, T., Chiavazza, E., Daniele, P.G., Minella, M., Isaia, M., Brigante, M., and Vione, D.: Properties of the humic-like material arising from the photo-transformation of L-tyrosine, Sci. Total Environ., 434–444, https://doi.org/10.1016/j.scitotenv.2015.12.047, 2016.

Bianco, A., Minella, M., De Laurentiis, E., Maurino, V., Minero, C., and Vione, D.: Photochemical generation of photoactive compounds with fulvic-like and humic-like fluorescence in aqueous solution, Chemosphere, 111, 529–536, https://doi.org/10.1016/j.chemosphere.2014.04.035, 2014.

Bianco, A., Riva, M., Baray, J.-L., Ribeiro, M., Chaumerliac, N., George, C., Bridoux, M., and Deguillaume, L.: Chemical characterization of cloud water collected at Puy de Dôme by FT-ICR MS reveals the presence of SOA components, ACS Earth Space Chem., 3, 2076–2087, https://doi.org/10.1021/acsearthspacechem.9b00153, 2019.

Bianco, A., Passananti, M., Brigante, M., and Mailhot, G.: Photochemistry of the cloud aqueous phase: a review, Molecules, 25, 423, https://doi.org/10.3390/molecules25020423, 2020.

Birks, J.B.: Organic Molecular Photophysics, John Wiley & Sons, 1973.

Blando, J. D. and Turpin, B. J.: Secondary organic aerosol formation in cloud and fog droplets: a literature evaluation of plausibility, Atmos. Environ., 34, 1623−1632, https://doi.org/10.1016/S1352-2310(99)00392-1, 2000.

564 Bond, T. C., Streets, D. G., Yarber, K. F., Nelson, S. M., Woo, J-H., and Klimont, Z.: A technology-based global inventory of
565 black and organic carbon emissions from combustion, J. Geophys. Res., 109, https://doi.org/10.1029/2003JD003697, 2004.
566
567 Brezonik, P. L. and Fulkerson-Brekken, J.: Nitrate-induced photolysis in natural waters: controls on concentrations of hydroxyl
568 radical photo-intermediates by natural scavenging agents, Environ. Sci. Technol., 32, 3004−3010,
569 https://doi.org/10.1021/es9802908, 1998.
570
571 Canonica, S., Hellrung, B., and Wirz, J.: Oxidation of phenols by triplet aromatic ketones in aqueous solution, J. Phys. Chem,
572 104, 1226–1232, https://doi.org/10.1021/jp9930550, 2000.
573
574 Canonica, S., Jans, U., Stemmler, K., and Hoigne, J.: Transformation kinetics of phenols in water: photosensitization by
575 dissolved natural organic material and aromatic ketones, Environ. Sci. Technol., 29, 1822–1831,
576 https://doi.org/10.1021/es00007a020, 1995.
577
578 Chang, J. L. and Thompson, J. E.: Characterization of colored products formed during irradiation of aqueous solutions
579 containing H_2O_2 and phenolic compounds, Atmos. Environ., 44, 541−551, https://doi.org/10.1016/j.atmosenv.2009.10.042,
580 2010.
581
582 Chen, Y., Li, N., Li, X., Tao, Y., Luo, S., Zhao, Z., Ma, S., Huang, H., Chen, Y., Ye, Z., and Ge, X.: Secondary organic aerosol
583 formation from [3]C*-initiated oxidation of 4-ethylguaiacol in atmospheric aqueous-phase, Sci. Total Environ., 723, 137953,
584 https://doi.org/10.1016/j.scitotenv.2020.137953, 2020.
585
586 Chu, L. and Anastasio, C.: Quantum yields of hydroxyl radical and nitrogen dioxide from the photolysis of nitrate on ice, J.
587 Phys. Chem. A, 107, 9594−9602, https://doi.org/10.1021/jp0349132, 2003.
588
589 Collett, J. L. Jr., Hoag, K. J., Sherman, D. E., Bator, A., and Richards, L. W.: Spatial and temporal variations in San Joaquin
590 Valley fog chemistry, Atmos. Environ., 33, 129−140, https://doi.org/10.1016/S1352-2310(98)00136-8, 1998.
591
592 De Haan, D. O., Corrigan, A. L., Tolbert, M. A., Jimenez, J. L., Wood, S. E., and Turley, J. J.: Secondary organic aerosol
593 formation by self-reactions of methylglyoxal and glyoxal in evaporating droplets, Environ. Sci. Technol., 43, 8184−8190,
594 https://doi.org/10.1021/es902152t, 2009.
595
596 De Haan, D. O., Hawkins, L. N., Kononenko, J. A., Turley, J. J., Corrigan, A. L., Tolbert, M. A., and Jimenez, J. L.: Formation
597 of nitrogen-containing oligomers by methylglyoxal and amines in simulated evaporating cloud droplets, Environ. Sci. Technol.,
598 45, 984−991, https://doi.org/10.1021/es102933x, 2011.
599
600 De Haan, D.O., Pajunoja, A., Hawkins, L. N., Welsh, H.G., Jimenez, N. G., De Loera, A., Zauscher, M., Andretta, A. D.,
601 Joyce, B. W., De Haan, A. C., Riva, M., Cui, T., Surratt, J. D., Cazaunau, M., Formenti, P., Gratien, A., Pangui, E., and
602 Doussin, J-F.: Methylamine's effects on methylglyoxal-containing aerosol: chemical, physical, and optical changes, ACS
603 Earth Space Chem., 3, 1706–1716, https://doi.org/10.1021/acsearthspacechem.9b00103, 2019.
604
605 De Laurentiis, E., Socorro, J., Vione, D., Quivet, E., Brigante, M., Mailhot, G., Wortham, H., and Gligorovski, S.:
606 Phototransformation of 4-phenoxyphenol sensitised by 4-carboxybenzophenone: Evidence of new photochemical pathways in
607 the bulk aqueous phase and on the surface of aerosol deliquescent particles, Atmos. Environ., 81, 569–578,
608 https://doi.org/10.1016/j.atmosenv.2013.09.036, 2013a.
609
610 De Laurentiis, E., Sur, B., Pazzi, M., Maurino, V., Minero, C., Mailhot, G., Brigante, M., and Vione, D.: Phenol transformation
611 and dimerisation, photosensitised by the triplet state of 1-nitronaphthalene: a possible pathway to humic-like substances
612 (HULIS) in atmospheric waters, Atmos. Environ., 70, 318–327, https://doi.org/10.1016/j.atmosenv.2013.01.014, 2013b.
613

Desyaterik, Y., Sun, Y., Shen, X., Lee, T., Wang, X., Wang, T., and Collett, J. L. Jr.: Speciation of "brown" carbon in cloud water impacted by agricultural biomass burning in eastern China, J. Geophys. Res. Atmos., 118, 7389–7399, https://doi.org/10.1002/jgrd.50561, 2013.

Du, Y., Fu, Q. S., Li, Y., and Su, Y.: Photodecomposition of 4-chlorophenol by reactive oxygen species in UV/air system, J. Hazard. Mater., 186, 491–496, https://doi.org/10.1016/j.jhazmat.2010.11.023, 2011.

Dzengel, J., Theurich, J., and Bahnemann, D. W.: Formation of nitroaromatic compounds in advanced oxidation processes: photolysis versus photocatalysis, Environ. Sci. Technol., 33, 294–300, https://doi.org/10.1021/es980358j, 1999.

Ervens, B., Turpin, B. J., and Weber, R. J.: Secondary organic aerosol formation in cloud droplets and aqueous particles (aqSOA): a review of laboratory, field and model studies, Atmos. Chem. Phys., 11, 11069−11102, https://doi.org/10.5194/acp-11-11069-2011, 2011.

Fischer, M. and Warneck, P.: Photodecomposition of nitrite and undissociated nitrous acid in aqueous solution, J. Phys. Chem., 100, 18749−18756, https://doi.org/10.1021/jp961692+, 1996.

Fleming, L. T., Lin, P., Laskin, A., Laskin, J., Weltman, R., Edwards, R. D., Arora, N. K., Yadav, A., Meinardi, S., Blake, D. R., Pillarisetti, A., Smith, K. R., and Nizkorodov, S. A.: Molecular composition of particulate matter emissions from dung and brushwood burning household cookstoves in Haryana, India, Atmos. Chem. Phys., 18, 2461–2480, https://doi.org/10.5194/acp-18-2461-2018, 2018.

Foote, C.S.: Definition of type I and type II photosensitized oxidation, Photochem. Photobiol., 54, 659, https://doi.org/10.1111/j.1751-1097.1991.tb02071.x, 1991.

Galloway, M. M., Chhabra, P. S., Chan, A. W. H., Surratt, J. D., Flagan, R. C., Seinfeld, J. H., and Keutsch, F. N.: Glyoxal uptake on ammonium sulphate seed aerosol: reaction products and reversibility of uptake under dark and irradiated conditions, Atmos. Chem. Phys., 9, 3331−3345, https://doi.org/10.5194/acp-9-3331-2009, 2009.

Gelencsér, A., Hoffer, A., Kiss, G., Tombácz, E., Kurdi, R., and Bencze, L.: In-situ formation of light-absorbing organic matter in cloud water, J. Atmos. Chem., 45, 25–33, https://doi.org/10.1023/A:1024060428172, 2003.

Gen, M., Huang, D. D., and Chan, C. K.: Reactive uptake of glyoxal by ammonium-containing salt particles as a function of relative humidity, Environ. Sci. Technol., 52, 6903−6911, https://doi.org/10.1021/acs.est.8b00606, 2018.

Gen, M., Zhang, R., Huang, D. D., Li, Y., and Chan, C. K.: Heterogeneous SO_2 oxidation in sulfate formation by photolysis of particulate nitrate, Environ. Sci. Technol. Lett., 6, 86–91, https://doi.org/10.1021/acs.estlett.8b00681, 2019a.

Gen, M., Zhang, R., Huang, D. D., Li, Y., and Chan, C. K.: Heterogeneous oxidation of SO_2 in sulfate production during nitrate photolysis at 300 nm: effect of pH, relative humidity, irradiation intensity, and the presence of organic compounds, Environ. Sci. Technol., 53, 8757–8766, https://doi.org/10.1021/acs.est.9b01623, 2019b.

George, C., Ammann, M., D'Anna, B., Donaldson, D. J., and Nizkorodov, S.A.: Heterogeneous photochemistry in the atmosphere, Chem. Rev., 115, 4218–4258, https://doi.org/10.1021/cr500648z, 2015.

George, C., Brüggemann, M., Hayeck, N., Tinel, L., and Donaldson, J.: Interfacial photochemistry: physical chemistry of gas-liquid interfaces, in: Developments in Physical & Theoretical Chemistry, edited by: Faust, J. A. and House, J. E., Elsevier, 435−457, https://doi.org/10.1016/B978-0-12-813641-6.00014-5, 2018.

Gilardoni, S., Massoli, P., Paglione, M., Giulianelli, L., Carbone, C., Rinaldi, M., Decesari, S., Sandrini, S., Costabile, F., Gobbi, G.P., Pietrogrande, M.C., Visentin, M., Scotto, F., Fuzzi, S., and Facchini, M.C.: Direct observation of aqueous secondary organic aerosol from biomass-burning emissions, PNAS., 113, 10013–10018, https://doi.org/10.1073/pnas.1602212113, 2016.

Giulianelli, L., Gilardoni, S., Tarozzi, L., Rinaldi, M., Decesari, S., Carbone, C., Facchini, M. C., and Fuzzi, S.: Fog occurrence and chemical composition in the Po valley over the last twenty years, Atmos. Environ., 98, 394–401, https://doi.org/10.1016/j.atmosenv.2014.08.080, 2014.

Goldstein, S. and Czapski, G.: Kinetics of nitric oxide autoxidation in aqueous solution in the absence and presence of various reductants. The nature of the oxidizing intermediates, J. Am. Chem. Soc., 117, 12078–12084, https://doi.org/10.1021/ja00154a007, 1995.

Grosjean, D.: Reactions of o-cresol and nitrocresol with nitrogen oxides (NO_x) in sunlight and with ozone–nitrogen dioxide mixtures in the dark, Environ. Sci. Technol., 19, 968–974, https://doi.org/10.1021/es00140a014, 1985.

Herrmann, H.: On the photolysis of simple anions and neutral molecules as sources of O^-/OH, SO_x^- and Cl in aqueous solution, Phys. Chem. Chem. Phys., 9, 3935-3964, https://doi.org/10.1039/B618565G, 2007.

Herrmann, H., Hoffmann, D., Schaefer, T., Bräuer, P., and Tilgner, A.: Tropospheric aqueous-phase free-radical chemistry: radical sources, spectra, reaction kinetics and prediction tools, Chem Phys Chem., 11, 3796−3822, https://doi.org/10.1002/cphc.201000533, 2010.

Hoffer, A., Kiss, G., Blazsó, M., and Gelencsér, A.: Chemical characterization of humic-like substances (HULIS) formed from a lignin-type precursor in model cloud water, Geophys. Res. Lett., 31, https://doi.org/10.1029/2003GL018962, 2004.

Hoffmann, E. H., Tilgner, A., Wolke, R., Böge, O., Walter, A., and Herrmann, H.: Oxidation of substituted aromatic hydrocarbons in the tropospheric aqueous phase: kinetic mechanism development and modelling, Phys. Chem. Chem. Phys., 20, 10960–10977, https://doi.org/10.1039/C7CP08576A, 2018.

Holčapek, M., Jirásko, R., and Lísa, M.: Basic rules for the interpretation of atmospheric pressure ionization mass spectra of small molecules, J. Chromatogr. A, 1217, 3908–3921, https://doi.org/10.1016/j.chroma.2010.02.049, 2010.

Huang, D. D., Zhang, Q., Cheung, H. H. Y., Yu, L., Zhou, S., Anastasio, C., Smith, J. D., and Chan, C. K.: Formation and evolution of aqSOA from aqueous-phase reactions of phenolic carbonyls: comparison between ammonium sulfate and ammonium nitrate solutions, Environ. Sci. Technol., 52, 9215–9224, https://doi.org/10.1021/acs.est.8b03441, 2018.

Huang, R.-J., Zhang, Y., Bozzetti, C., Ho, K.-F., Cao, J.-J., Han, Y., Daellenbach, K. R., Slowik, J. G., Platt, S. M., Canonaco, F., Zotter, P., Wolf, R., Pieber, S. M., Bruns, E. A., Crippa, M., Ciarelli, G., Piazzalunga, A., Schwikowski, M., Abbaszade, G., Schnelle-Kreis, J., Zimmermann, R., An, Z., Szidat, S., Baltensperger, U., El Haddad, I., and Prévôt, A. S. H.: High secondary aerosol contribution to particulate pollution during haze events in China, Nature, 514, 218–222, https://doi.org/10.1038/nature13774, 2014.

Huang, X. H. H., Ip, H. S. S., and Yu, J. Z.: Secondary organic aerosol formation from ethylene in the urban atmosphere of Hong Kong: a multiphase chemical modeling study, J. Geophys. Res., 116, D03206, https://doi.org/10.1029/2010JD014121, 2011.

Jacobson, M. Z.: Isolating nitrated and aromatic aerosols and nitrated aromatic gases as sources of ultraviolet light absorption, J. Geophys. Res., 104, 3527–3542, https://doi.org/10.1029/1998JD100054, 1999.

713 Jiang, W., Misovich, M. V., Hettiyadura, A. P. S., Laskin, A., McFall, A. S., Anastasio, C., and Zhang, Q.: Photosensitized
714 reactions of a phenolic carbonyl from wood combustion in the aqueous phase—chemical evolution and light absorption
715 properties of aqSOA, Environ. Sci. Technol., 55, 5199–5211, https://doi.org/10.1021/acs.est.0c07581, 2021.
716
717 Jimenez, J. L., Canagaratna, M. R., Donahue, N. M., Prevot, A. S. H., Zhang, Q., Kroll, J. H., DeCarlo, P. F., Allan, J. D., Coe,
718 H., Ng, N. L., Aiken, A. C., Docherty, K. S., Ulbrich, I. M., Grieshop, A. P., Robinson, A. L., Duplissy, J., Smith, J. D., Wilson,
719 K. R., Lanz, V. A., Hueglin, C., Sun, Y. L., Tian, J., Laaksonen, A., Raatikainen, T., Rautiainen, J., Vaattovaara, P., Ehn, M.,
720 Kulmala, M., Tomlinson, J. M., Collins, D. R., Cubison, M. J., Dunlea, E., J., Huffman, J. A., Onasch, T. B., Alfarra, M. R.,
721 Williams, P. I., Bower, K., Kondo, Y., Schneider, J., Drewnick, F., Borrman, S., Weimer, S., Demerjian, K., Salcedo, D.,
722 Cottrell, L., Griffin, R., Takami, A., Miyoshi, T., Hatakeyama, S., Shimono, A., Sun, J. Y., Zhang, Y. M., Dzepina, K., Kimmel,
723 J. R., Sueper, D., Jayne, J. T., Herndon, S. C., Trimborn, A. M., Williams, L. R., Wood, E. C., Middlebrook, A. M., Kolb, C.
724 E., Baltensperger, U., and Worsnop, D. R.: Evolution of organic aerosols in the atmosphere, Science, 326, 1525–1529,
725 https://doi.org/10.1126/science.1180353, 2009.
726
727 Kahnt, A., Behrouzi, S., Vermeylen, R., Shalamzari, M. S., Vercauteren, J., Roekens, E., Claeys, M., and Maenhaut, W.: One-
728 year study of nitro-organic compounds and their relation to wood burning in PM$_{10}$ aerosol from a rural site in Belgium, Atmos.
729 Environ., 81, 561−568, https://doi.org/10.1016/j.atmosenv.2013.09.041, 2013.
730
731 Kaur, R. and Anastasio, C.: First measurements of organic triplet excited states in atmospheric waters, Environ. Sci. Technol.,
732 52, 5218–5226, https://doi.org/10.1021/acs.est.7b06699, 2018.
733
734 Kaur, R., Labins, J. R., Helbock, S. S., Jiang, W., Bein, K. J., Zhang, Q., and Anastasio, C.: Photooxidants from brown carbon
735 and other chromophores in illuminated particle extracts, Atmos. Chem. Phys., 19, 6579–6594, https://doi.org/10.5194/acp-19-
736 6579-2019, 2019.
737
738 Kebarle, P.: A brief overview of the present status of the mechanisms involved in electrospray mass spectrometry, J. Mass
739 Spectrom., 35, 804−817, https://doi.org/10.1002/1096-9888(200007)35:7<804::AID-JMS22>3.0.CO;2-Q, 2000.
740
741 Kim, D.-h., Lee, J., Ryu, J., Kim, K., and Choi, W.: Arsenite oxidation initiated by the UV photolysis of nitrite and nitrate,
742 Environ. Sci. Technol., 48, 4030−4037, https://doi.org/10.1021/es500001q, 2014.
743
744 Kitanovski, Z., Čusak, A., Grgić, I., and Claeys, M.: Chemical characterization of the main products formed through aqueous-
745 phase photonitration of guaiacol, Atmos. Meas. Tech., 7, 2457–2470, https://doi.org/10.5194/amt-7-2457-2014, 2014.
746
747 Klodt, A. L., Romonosky, D. E., Lin, P., Laskin, J., Laskin, A., and Nizkorodov, S. A.: Aqueous photochemistry of secondary
748 organic aerosol of α-pinene and α-humulene in the presence of hydrogen peroxide or inorganic salts, ACS Earth Space Chem.,
749 3, 12, 2736–2746, https://doi.org/10.1021/acsearthspacechem.9b00222, 2019.
750
751 Kobayashi, S. and Higashimura, H.: Oxidative polymerization of phenols revisited, Prog. Polym. Sci., 28, 1015–1048,
752 https://doi.org/10.1016/S0079-6700(03)00014-5, 2003.
753
754 Kourtchev, I., Fuller, S. J., Giorio, C., Healy, R. M., Wilson, E., O'Connor, I., Wenger, J. C., McLeod, M., Aalto, J.,
755 Ruuskanen, T. M., Maenhaut, W., Jones, R., Venables, D. S., Sodeau, J. R., Kulmala, M., and Kalberer, M.: Molecular
756 composition of biogenic secondary organic aerosols using ultrahigh-resolution mass spectrometry: comparing laboratory and
757 field studies, Atmos. Chem. Phys., 14, 2155−2167, https://doi.org/10.5194/acp-14-2155-2014, 2014.
758
759 Kroflič, A., Anders, J., Drventić, I., Mettke, P., Böge, O., Mutzel, A., Kleffmann, J., and Herrmann, H.: Guaiacol nitration in
760 a simulated atmospheric aerosol with an emphasis on atmospheric nitrophenol formation mechanisms, ACS Earth Space Chem.,
761 5, 1083−1093, https://doi.org/10.1021/acsearthspacechem.1c00014, 2021.
762

Kroflič, A., Grilc, M., and Grgić, I.: Unraveling pathways of guaiacol nitration in atmospheric waters: nitrite, a source of reactive nitronium ion in the atmosphere, Environ. Sci. Technol., 49, 9150–9158, https://doi.org/10.1021/acs.est.5b01811, 2015.

Kroll, J. H., Donahue, N. M., Jimenez, J. L., Kessler, S. H., Canagaratna, M. R., Wilson, K. R., Altieri, K. E., Mazzoleni, L. R., Wozniak, A. S., Bluhm, H., Mysak, E. R., Smith, J. D., Kolb, C. E., and Worsnop, D. R.: Carbon oxidation state as a metric for describing the chemistry of atmospheric organic aerosol, Nat. Chem., 3, 133–139, https://doi.org/10.1038/nchem.948, 2011.

Kruve, A., Kaupmees, K., Liigand, J., and Leito, I.: Negative electrospray ionization via deprotonation: predicting the ionization efficiency, Anal. Chem., 86, 4822–4830, https://doi.org/10.1021/ac404066v, 2014.

Laskin, A., Laskin, J., and Nizkorodov, S. A.: Chemistry of atmospheric brown carbon, Chem. Rev., 115, 4335–4382, https://doi.org/10.1021/cr5006167, 2015.

Laskin, J., Laskin, A., Nizkorodov, S. A., Roach, P., Eckert, P., Gilles, M. K., Wang, B., Lee, H. J., and Hu, Q.: Molecular selectivity of brown carbon chromophores, Environ. Sci. Technol., 48, 12047–12055, https://doi:10.1021/es503432r, 2014.

Lathioor, E. C., Leigh, W. J., and St. Pierre, M. J.: Geometrical effects on intramolecular quenching of aromatic ketone (π,π*) triplets by remote phenolic hydrogen abstraction, J. Am. Chem. Soc., 121, 11984–11992, https://pubs.acs.org/doi/abs/10.1021/ja991207z, 1999.

LeClair, J. P., Collett, J. L., and Mazzoleni, L. R.: Fragmentation analysis of water-soluble atmospheric organic matter using ultrahigh-resolution FT-ICR mass spectrometry, Environ. Sci. Technol., 46, 4312–4322, https://doi.org/10.1021/es203509b, 2012.

Lee, A. K. Y., Herckes, P., Leaitch, W. R., Macdonald, A. M., and Abbatt, J. P. D.: Aqueous OH oxidation of ambient organic aerosol and cloud water organics: Formation of highly oxidized products, Geophys. Res. Lett., 38, L11805, https://doi.org/10.1029/2011GL047439, 2011.

Lee, A. K. Y., Zhao, R., Li, R., Liggio, J., Li, S.-M., and Abbatt, J. P. D.: Formation of light absorbing organo-nitrogen species from evaporation of droplets containing glyoxal and ammonium sulfate, Environ. Sci. Technol., 47, 12819−12826, https://doi.org/10.1021/es402687w, 2013.

Lee, H. J., Aiona, P. K., Laskin, A., Laskin, J., and Nizkorodov, S. A.: Effect of solar radiation on the optical properties and molecular composition of laboratory proxies of atmospheric brown carbon, Environ. Sci. Technol., 48, 10217–10226, https://doi.org/10.1021/es502515r, 2014.

Lee, P. C. C. and Rodgers, M. A. J.: Laser flash photokinetic studies of Rose Bengal sensitized photodynamic interactions of nucleotides and DNA, Photochem. Photobiol., 45, 79–86, https://doi.org/10.1111/j.1751-1097.1987.tb08407.x, 1987.

Leito, I., Herodes, K., Huopolainen, M., Virro, K., Künnapas, A., Kruve, A., and Tanner, R.: Towards the electrospray ionization mass spectrometry ionization efficiency scale of organic compounds, Rapid Commun. Mass Sp., 22, 379–384, https://doi.org/10.1002/rcm.3371, 2008.

Li, F., Tang, S., Tsona, N. T., and Du, L.: Kinetics and mechanism of OH-induced α-terpineol oxidation in the atmospheric aqueous phase, Atmos. Environ., 237, 117650, https://doi.org/10.1016/j.atmosenv.2020.117650, 2020.

Li, P., Li, X., Yang, C., Wang, X., Chen, J., and Collett, J. L. Jr.: Fog water chemistry in Shanghai, Atmos. Environ., 45, 4034−4041, https://doi.org/10.1016/j.atmosenv.2011.04.036, 2011.

813 Li, Y. J., Huang, D. D., Cheung, H. Y., Lee, A. K. Y., and Chan, C. K.: Aqueous-phase photochemical oxidation and direct
814 photolysis of vanillin - a model compound of methoxy phenols from biomass burning, Atmos. Chem. Phys., 14, 2871−2885,
815 https://doi.org/10.5194/acp-14-2871-2014, 2014.

817 Liang, Z., Zhang, R., Gen, M., Chu, Y., and Chan, C. K.: Nitrate photolysis in mixed sucrose–nitrate–sulfate particles at
818 different relative humidities, J. Phys. Chem. A, 125, 3739–3747, https://doi.org/10.1021/acs.jpca.1c00669, 2021.

820 Liigand, P., Kaupmees, K., Haav, K., Liigand, J., Leito, I., Girod, M., Antoine, R., and Kruve, A.: Think negative: finding the
821 best electrospray ionization/MS mode for your analyte, Anal. Chem., 89, 5665–5668,
822 https://doi.org/10.1021/acs.analchem.7b00096, 2017.

824 Lim, Y. B., Tan, Y., Perri, M. J., Seitzinger, S. P., and Turpin, B. J.: Aqueous chemistry and its role in secondary organic
825 aerosol (SOA) formation, Atmos. Chem. Phys., 10, 10521−10539, https://doi.org/10.5194/acp-10-10521-2010, 2010.

827 Lin, P., Bluvshtein, N., Rudich, Y., Nizkorodov, S. A., Laskin, J., and Laskin, A.: Molecular chemistry of atmospheric brown
828 carbon inferred from a nationwide biomass burning event, Environ. Sci. Tech., 51, 11561–
829 11570, https://doi.org/10.1021/acs.est.7b02276, 2017.

831 Lin, P., Fleming, L. T., Nizkorodov, S. A., Laskin, J., and Laskin, A.: Comprehensive molecular characterization of
832 atmospheric brown carbon by high resolution mass spectrometry with electrospray and atmospheric pressure photoionization,
833 Anal. Chem., 90, 12493–12502, https://doi.org/10.1021/acs.analchem.8b02177, 2018.

835 Lin, P., Yu, J. Z., Engling, G., and Kalberer, M.: Organosulfates in humic-like substance fraction isolated from aerosols at
836 seven locations in East Asia: a study by ultra-high-resolution mass spectrometry, Environ. Sci. Technol., 46, 13118–13127,
837 https://doi.org/10.1021/es303570v, 2012.

839 Liu, C., Liu, J., Liu, Y., Chen, T., and He, H.: Secondary organic aerosol formation from the OH-initiated oxidation of guaiacol
840 under different experimental conditions, Atmos. Environ., 207, 30–37, https://doi.org/10.1016/j.atmosenv.2019.03.021, 2019.

842 Lobodin, V. V., Marshall, A. G., and Hsu, C. S.: Compositional space boundaries for organic compounds, Anal. Chem., 84,
843 3410–3416, https://doi.org/10.1021/ac300244f, 2012.

845 Loisel, G., Mekic, M., Liu, S., Song, W., Jiang, B., Wang, Y., Deng, H., and Gligorovski, S.: Ionic strength effect on the
846 formation of organonitrate compounds through photochemical degradation of vanillin in liquid water of aerosols, Atmos.
847 Environ., 246, 118140, https://doi.org/10.1016/j.atmosenv.2020.118140, 2021.

849 Ma, L., Guzman, C., Niedek, C., Tran, T., Zhang, Q., and Anastasio, C.: Kinetics and mass yields of aqueous secondary organic
850 aerosol from highly substituted phenols reacting with a triplet excited state, Environ. Sci. Technol., 55, 5772–5781,
851 https://doi.org/10.1021/acs.est.1c00575, 2021.

853 Mabato, B. R. G., Gen, M., Chu, Y., and Chan, C. K.: Reactive uptake of glyoxal by methylaminium-containing salts as a
854 function of relative humidity, ACS Earth Space Chem., 3, 150–157, https://doi.org/10.1021/acsearthspacechem.8b00154, 2019.

856 Machado, F. and Boule, P.: Photonitration and photonitrosation of phenolic derivatives induced in aqueous solution by
857 excitation of nitrite and nitrate ions, J. Photochem. Photobiol. A: Chem., 86, 73–80, https://doi.org/10.1016/1010-
858 6030(94)03946-R, 1995.

860 Mack, J. and Bolton, J. R.: Photochemistry of nitrite and nitrate in aqueous solution: a review, J. Photochem. Photobiol. A,
861 128, 1–13, https://doi.org/10.1016/S1010-6030(99)00155-0, 1999.

Mazzoleni, L. R., Saranjampour, P., Dalbec, M. M., Samburova, V., Hallar, A. G., Zielinska, B., Lowenthal, D. H., and Kohl, S.: Identification of water-soluble organic carbon in non-urban aerosols using ultrahigh-resolution FT-ICR mass spectrometry: organic anions, Environ. Chem., 9, 285−297, https://doi.org/10.1071/EN11167, 2012.

McFall, A. S., Johnson, A. W., and Anastasio, C.: Air–water partitioning of biomass-burning phenols and the effects of temperature and salinity, Environ. Sci. Technol., 54, 3823–3830, https://doi.org/10.1021/acs.est.9b06443, 2020.

McNally, A. M., Moody, E. C., and McNeill, K.: Kinetics and mechanism of the sensitized photodegradation of lignin model compounds, Photochem. Photobiol. Sci., 4, 268−274, https://doi.org/10.1039/B416956E, 2005.

Minella, M., Romeo, F., Vione, D., Maurino, V., and Minero, C.: Low to negligible photoactivity of lake-water matter in the size range from 0.1 to 5 μm, Chemosphere, 83, 1480–1485, https://doi.org/10.1016/j.chemosphere.2011.02.093, 2011.

Minero, C., Bono, F., Rubertelli, F., Pavino, D., Maurino, V., Pelizzetti, E., and Vione, D.: On the effect of pH in aromatic photonitration upon nitrate photolysis, Chemosphere, 66, 650−656, https://doi.org/10.1016/j.chemosphere.2006.07.082, 2007.

Misovich, M. V., Hettiyadura, A. P. S., Jiang, W., Zhang, Q., and Laskin, A.: Molecular-level study of the photo-oxidation of aqueous-phase guaiacyl acetone in the presence of $^3C^*$: formation of brown carbon products, ACS Earth Space Chem., 5, 1983−1996, https://doi.org/10.1021/acsearthspacechem.1c00103, 2021.

Mohr, C., Lopez-Hilfiker, F. D., Zotter, P., Prévôt, A. S. H., Xu, L., Ng, N. L., Herndon, S. C., Williams, L. R., Franklin, J. P., Zahniser, M. S., Worsnop, D. R., Knighton, W. B., Aiken, A. C., Gorkowski, K. J., Dubey, M. K., Allan, J. D., and Thornton, J. A.: Contribution of nitrated phenols to wood burning brown carbon light absorption in Detling, United Kingdom during winter time, Environ. Sci. Technol., 47, 6316–6324, https://doi.org/10.1021/es400683v, 2013.

Munger, J. W., Jacob, D. J., Waldman, J. M., and Hoffmann, M. R.: Fogwater chemistry in an urban atmosphere, J. Geophys. Res. Oceans, 88, 5109–5121, https://doi.org/10.1029/JC088iC09p05109, 1983.

Neumann, M. G., De Groote, R. A. M. C., and Machado, A. E. H.: Flash photolysis of lignin: Part 1. Deaerated solutions of dioxane-lignin, Polym. Photochem., 7, 401–407, https://doi.org/10.1016/0144-2880(86)90007-2, 1986a.

Neumann, M. G., De Groote, R. A. M. C., and Machado, A. E. H.: Flash photolysis of lignin: II. Oxidative photodegradation of dioxane-lignin, Polym. Photochem., 7, 461–468, https://doi.org/10.1016/0144-2880(86)90015-1, 1986b.

Ning, C., Gao, Y., Zhang, H., Yu, H., Wang, L., Geng, N., Cao, R., and Chen, J.: Molecular characterization of dissolved organic matters in winter atmospheric fine particulate matters ($PM_{2.5}$) from a coastal city of northeast China, Sci. Total Environ., 689, 312–321, https://doi.org/10.1016/j.scitotenv.2019.06.418, 2019.

Nolte, C. G., Schauer, J. J., Cass, G. R., and Simoneit, B. R. T.: Highly polar organic compounds present in wood smoke and in the ambient atmosphere, Environ. Sci. Technol., 35, 1912−1919, https://doi.org/10.1021/es001420r, 2001.

Nozière, B., Dziedzic, P., and Córdova, A.: Products and kinetics of the liquid-phase reaction of glyoxal catalyzed by ammonium ions (NH_4^+), J. Phys. Chem. A, 113, 231−237, https://doi.org/10.1021/jp8078293, 2009.

Nozière, B., Dziedzic, P., and Córdova, A.: Inorganic ammonium salts and carbonate salts are efficient catalysts for aldol condensation in atmospheric aerosols, Phys. Chem. Chem. Phys., 12, 3864−3872, https://doi.org/10.1039/B924443C, 2010.

Nozière, B., Fache, F., Maxut, A., Fenet, B., Baudouin, A., Fine, L., and Ferronato, C.: The hydrolysis of epoxides catalyzed by inorganic ammonium salts in water: kinetic evidence for hydrogen bond catalysis, Phys. Chem. Chem. Phys., 20, 1583−1590, https://doi.org/10.1039/C7CP06790A, 2018.

Pang, H., Zhang, Q., Lu, X. H., Li, K. , Chen, H., Chen, J. , Yang, X., Ma, Y., Ma, J., and Huang, C.: Nitrite-mediated photooxidation of vanillin in the atmospheric aqueous phase, Environ. Sci. Technol., 53, 14253−14263, https://doi.org/10.1021/acs.est.9b03649, 2019a.

Pang, H., Zhang, Q., Wang, H., Cai, D., Ma, Y., Li, L., Li, K., Lu, X., Chen, H., Yang, X., and Chen, J.: Photochemical aging of guaiacol by Fe(III)-oxalate complexes in atmospheric aqueous phase, Environ. Sci. Technol., 53, 127−136, https://doi.org/10.1021/acs.est.8b04507, 2019b.

Perry, R. H., Cooks, R. G., and Noll, R. J.: Orbitrap mass spectrometry: instrumentation, ion motion and applications, Mass Spectrom. Rev., 27, 661–699, https://doi.org/10.1002/mas.20186, 2008.

Powelson, M. H., Espelien, B. M., Hawkins, L. N., Galloway, M. M., and De Haan, D. O.: Brown carbon formation by aqueous-phase carbonyl compound reactions with amines and ammonium sulfate, Environ. Sci. Technol., 48, 985−993, https://doi.org/10.1021/es4038325, 2014.

Pye, H., Nenes, A., Alexander, B., Ault, A. P., Barth, M. C., Clegg, S. L., Collett, J. L. Jr., Fahey, K. M., Hennigan, C. J., Herrmann, H., Kanakidou, M., Kelly, J. T., Ku, I-T., McNeill, V. F., Riemer, N., Schaefer, T., Shi, G., Tilgner, A., Walker, J. T., Wang, T., Weber, R., Xing, J., Zaveri, R. A., and Zuend, A.: The acidity of atmospheric particles and clouds, Atmos. Chem. Phys., 20, 4809–4888, https://doi.org/10.5194/acp-20-4809-2020, 2020.

Qi, L., Chen, M., Stefenelli, G., Pospisilova, V., Tong, Y., Bertrand, A., Hueglin, C., Ge, X., Baltensperger, U., Prévôt, A. S. H., and Slowik, J.G.: Organic aerosol source apportionment in Zurich using an extractive electrospray ionization time-of-flight mass spectrometer (EESI-TOF-MS) — Part 2: Biomass burning influences in winter, Atmos. Chem. Phys., 19, 8037–8062, https://doi.org/10.5194/acp-19-8037-2019, 2019.

Rogge, W. F., Hildemann, L. M., Mazurek, M. A., and Cass, G. R.: Sources of fine organic aerosol. 9. Pine, oak, and synthetic log combustion in residential fireplaces, Environ. Sci. Technol., 32, 13−22, https://doi.org/10.1021/es960930b, 1998.

Romonosky, D. E., Li, Y., Shiraiwa, M., Laskin, A., Laskin, J., and Nizkorodov, S. A.: Aqueous photochemistry of secondary organic aerosol of α-Pinene and α-Humulene oxidized with ozone, hydroxyl radical, and nitrate radical, J. Phys. Chem. A, 121, 1298–1309, https://doi.org/10.1021/acs.jpca.6b10900, 2017.

Scharko, N. K., Berke, A. E., and Raff, J. D.: Release of nitrous acid and nitrogen dioxide from nitrate photolysis in acidic aqueous solutions, Environ. Sci. Technol., 48, 20, 11991–1200, https://doi.org/10.1021/es503088x, 2014.

Schauer, J. J., Kleeman, M. J., Cass, G. R., and Simoneit, B. R. T.: Measurement of emissions from air pollution sources. 3. $C_1−C_{29}$ organic compounds from fireplace combustion of wood, Environ. Sci. Technol., 35, 1716−1728, https://doi.org/10.1021/es001331e, 2001.

Schmidt, A-C., Herzschuh, R., Matysik, F-M., and Engewald, W.: Investigation of the ionisation and fragmentation behaviour of different nitroaromatic compounds occurring as polar metabolites of explosives using electrospray ionisation tandem mass spectrometry, Rapid Commun. Mass Sp., 20, 2293–2302, https://doi.org/10.1002/rcm.2591, 2006.

Sedehi, N., Takano, H., Blasic, V. A., Sullivan, K. A., and De Haan, D. O.: Temperature- and pH-dependent aqueous-phase kinetics of the reactions of glyoxal and methylglyoxal with atmospheric amines and ammonium sulfate, Atmos. Environ., 77, 656−663, https://doi.org/10.1016/j.atmosenv.2013.05.070, 2013.

Shapiro, E. L., Szprengiel, J., Sareen, N., Jen, C. N., Giordano, M. R., and McNeill, V. F.: Light-absorbing secondary organic material formed by glyoxal in aqueous aerosol mimics, Atmos. Chem. Phys., 9, 2289−2300, https://doi.org/10.5194/acp-9-2289-2009, 2009.

963 Siegmann, K. and Sattler, K.: Formation mechanism for polycyclic aromatic hydrocarbons in methane flames, J. Chem. Phys.,
964 112, 698–709, https://doi.org/10.1063/1.480648, 2000.
965
966 Slikboer, S., Grandy, L., Blair, S. L., Nizkorodov, S. A., Smith, R. W., and Al-Abadleh, H. A.: Formation of light absorbing
967 soluble secondary organics and insoluble polymeric particles from the dark reaction of catechol and guaiacol with Fe(III),
968 Environ. Sci. Technol., 49, 7793–7801, https://doi.org/10.1021/acs.est.5b01032, 2015.
969
970 Smith, J. D., Kinney, H., and Anastasio, C.: Aqueous benzene-diols react with an organic triplet excited state and hydroxyl
971 radical to form secondary organic aerosol, Phys. Chem. Chem. Phys., 17, 10227–10237, https://doi.org/10.1039/C4CP06095D,
972 2015.
973
974 Smith, J. D., Kinney, H., and Anastasio, C.: Phenolic carbonyls undergo rapid aqueous photodegradation to form low-volatility,
975 light-absorbing products, Atmos. Environ., 126, 36−44, https://doi.org/10.1016/j.atmosenv.2015.11.035, 2016.
976
977 Smith, J. D., Sio, V., Yu, L., Zhang, Q., and Anastasio, C.: Secondary organic aerosol production from aqueous reactions of
978 atmospheric phenols with an organic triplet excited state, Environ. Sci. Technol., 48, 1049–1057,
979 https://doi.org/10.1021/es4045715, 2014.
980
981 Song, J., Li, M., Jiang, B., Wei, S., Fan, X., and Peng, P.: Molecular characterization of water-soluble humic like substances
982 in smoke particles emitted from combustion of biomass materials and coal using ultrahigh-resolution electrospray ionization
983 Fourier transform ion cyclotron resonance mass spectrometry, Environ. Sci. Technol., 52, 2575–2585,
984 https://doi.org/10.1021/acs.est.7b06126, 2018.
985
986 Sun, Y. L., Zhang, Q., Anastasio, C., and Sun, J.: Insights into secondary organic aerosol formed via aqueous-phase reactions
987 of phenolic compounds based on high resolution mass spectrometry, Atmos. Chem. Phys., 10, 4809−4822,
988 https://doi.org/10.5194/acp-10-4809-2010, 2010.
989
990 Teich, M., van Pinxteren, D., Kecorius, S., Wang, Z., and Herrmann, H.: First quantification of imidazoles in ambient aerosol
991 particles: potential photosensitizers, brown carbon constituents, and hazardous components, Environ. Sci. Technol., 50, 1166–
992 1173, https://doi.org/10.1021/acs.est.5b05474, 2016.
993
994 Teich, M., van Pinxteren, D., Wang, M., Kecorius, S., Wang, Z., Müller, T., Močnik, G., and Herrmann, H.: Contributions of
995 nitrated aromatic compounds to the light absorption of water-soluble and particulate brown carbon in different atmospheric
996 environments in Germany and China, Atmos. Chem. Phys., 17, 1653–1672, https://doi.org/10.5194/acp-17-1653-2017, 2017.
997
998 Tratnyek, P. G. and Hoigne, J.: Oxidation of substituted phenols in the environment: a QSAR analysis of rate constants for
999 reaction with singlet oxygen, Environ. Sci. Technol., 25, 1596−1604, https://doi.org/10.1021/es00021a011, 1991.
1000
1001 Turro, N., Ramamurthy, V., and Scaiano, J.C.: Modern Molecular Photochemistry, University Science Books, 2010.
1002
1003 Vione, D., Albinet, A., Barsotti, F., Mekic, M., Jiang, B., Minero, C., Brigante, M., and Gligorovski, S.: Formation of
1004 substances with humic-like fluorescence properties, upon photoinduced oligomerization of typical phenolic compounds
1005 emitted by biomass burning, Atmos. Environ., 206, 197−207, https://doi.org/10.1016/j.atmosenv.2019.03.005, 2019.
1006
1007 Vione, D., Maurino, V., Minero, C., and Pelizzetti, E.: Phenol photonitration upon UV irradiation of nitrite in aqueous solution
1008 I: effects of oxygen and 2-propanol, Chemosphere, 45, 893–902, https://doi.org/10.1016/S0045-6535(01)00035-2, 2001.
1009
1010 Vione, D., Maurino, V., Minero, C., and Pelizzetti, E.: Reactions induced in natural waters by irradiation of nitrate and nitrite
1011 ions, in: The Handbook of Environmental Chemistry Vol. 2M - Environmental Photochemistry Part II, Springer, Berlin,
1012 Heidelberg, Germany, 221−253, https://doi.org/10.1007/b138185, 2005.

Vione, D., Maurino, V., Minero, C., Pelizzetti, E., Harrison, M. A. J., Olariu, R., and Arsene, C.: Photochemical reactions in the tropospheric aqueous phase and on particulate matter, Chem. Soc. Rev., 35, 441−453, https://doi.org/10.1039/B510796M, 2006.

Volkamer, R., Ziemann, P. J., and Molina, M. J.: Secondary organic aerosol formation from acetylene (C_2H_2): seed effect on SOA yields due to organic photochemistry in the aerosol aqueous phase, Atmos. Chem. Phys., 9, 1907−1928, https://doi.org/10.5194/acp-9-1907-2009, 2009.

Wang, K., Huang, R-J., Brüggemann, M., Zhang, Y., Yang, L., Ni, H., Guo, J., Wang, M., Han, J., Bilde, M., Glasius, M., and Hoffmann, T.: Urban organic aerosol composition in eastern China differs from north to south: molecular insight from a liquid chromatography–mass spectrometry (Orbitrap) study, Atmos. Chem. Phys., 21, 9089–9104, https://doi.org/10.5194/acp-21-9089-2021, 2021.

Wang, X., Hayeck, N., Brüggemann, M., Yao, L., Chen, H., Zhang, C., Emmelin, C., Chen, J., George, C., and Wang, L.: Chemical characteristics of organic aerosols in Shanghai: a study by ultrahigh-performance liquid chromatography coupled with orbitrap mass spectrometry, J. Geophys. Res. Atmos., 122, 11703–11722, https://doi.org/10.1002/2017JD026930, 2017.

Xiao, H.-W., Wu, J.-F., Luo, L., Liu, C., Xie, Y.-J., and Xiao, H.-Y.: Enhanced biomass burning as a source of aerosol ammonium over cities in Central China in autumn, Environ. Pollut., 266, art. no. 115278, https://doi.org/10.1016/j.envpol.2020.115278, 2020.

Xie, Q., Su, S., Chen, S., Xu, Y., Cao, D., Chen, J., Ren, L., Yue, S., Zhao, W., Sun, Y., Wang, Z., Tong, H., Su, H., Cheng, Y., Kawamura, K., Jiang, G., Liu, C-Q., and Fu, P.: Molecular characterization of firework-related urban aerosols using Fourier transform ion cyclotron resonance mass spectrometry, Atmos. Chem. Phys., 20, 6803–6820, https://doi.org/10.5194/acp-20-6803-2020, 2020.

Yang, J., Au, W. C., Law, H., Lam, C. H., and Nah, T.: Formation and evolution of brown carbon during aqueous-phase nitrate-mediated photooxidation of guaiacol and 5-nitroguaiacol, Atmos. Environ., 254, 118401, https://doi.org/10.1016/j.atmosenv.2021.118401, 2021.

Yaws, C. L.: Handbook of vapor pressure: Volume 3: Organic compounds C_8 to C_{28}, Gulf Professional Publishing, USA, 1994.

Ye, Z., Qu, Z., Ma, S., Luo, S., Chen, Y., Chen, H., Chen, Y., Zhao, Z., Chen, M., and Ge, X.: A comprehensive investigation of aqueous-phase photochemical oxidation of 4-ethylphenol, Sci. Total Environ., 685, 976–985, https://doi.org/10.1016/j.scitotenv.2019.06.276, 2019.

Yee, L. D., Kautzman, K. E., Loza, C. L., Schilling, K. A., Coggon, M. M., Chhabra, P. S., Chan, M. N., Chan, A. W. H., Hersey, S. P., Crounse, J. D., Wennberg, P. O., Flagan, R. C., and Seinfeld, J. H.: Secondary organic aerosol formation from biomass burning intermediates: phenol and methoxyphenols, Atmos. Chem. Phys., 13, 8019−8043, https://doi.org/10.5194/acp-13-8019-2013, 2013.

Yu, G., Bayer, A. R., Galloway, M. M., Korshavn, K. J., Fry, C. G., and Keutsch, F. N.: Glyoxal in aqueous ammonium sulfate solutions: products, kinetics and hydration effects, Environ. Sci. Technol., 45, 6336−6342, https://doi.org/10.1021/es200989n, 2011.

Yu, L., Smith, J., Laskin, A., Anastasio, C., Laskin, J., and Zhang, Q.: Chemical characterization of SOA formed from aqueous-phase reactions of phenols with the triplet excited state of carbonyl and hydroxyl radical, Atmos. Chem. Phys., 14, 13801−13816, https://doi.org/10.5194/acp-14-13801-2014, 2014.

1062   Zhang, Q. and Anastasio, C.: Conversion of fogwater and aerosol organic nitrogen to ammonium, nitrate, and NO_x during
1063   exposure to simulated sunlight and ozone, Environ. Sci. Technol., 37, 3522–3530, https://doi.org/10.1021/es034114x, 2003.
1064
1065   Zhang, R., Gen, M., Fu, T-M., and Chan, C. K.: Production of formate via oxidation of glyoxal promoted by particulate nitrate
1066   photolysis, Environ. Sci. Technol., 55, 5711–5720, https://doi.org/10.1021/acs.est.0c08199, 2021.
1067
1068   Zhang, R., Gen, M., Huang, D. D., Li, Y., and Chan, C. K.: Enhanced sulfate production by nitrate photolysis in the presence
1069   of halide ions in atmospheric particles, Environ. Sci. Technol., 54, 3831–3839, https://dx.doi.org/10.1021/acs.est.9b06445,
1070   2020.
1071
1072   Zhao, R., Lee, A. K. Y., Huang, L., Li, X., Yang, F., and Abbatt, J. P. D.: Photochemical processing of aqueous atmospheric
1073   brown carbon, Atmos. Chem. Phys., 15, 6087–6100, https://doi.org/10.5194/acp-15-6087-2015, 2015.
1074
1075   Zhao, Y., Hallar, A. G., and Mazzoleni, L. R.: Atmospheric organic matter in clouds: exact masses and molecular formula
1076   identification using ultrahigh-resolution FT-ICR mass spectrometry, Atmos. Chem. Phys. 13, 12343–12362,
1077   https://doi.org/10.5194/acp-13-12343-2013, 2013.
1078
1079   Zhou, W., Mekic, M., Liu, J., Loisel, G., Jin, B., Vione, D., and Gligorovski, S.: Ionic strength effects on the photochemical
1080   degradation of acetosyringone in atmospheric deliquescent aerosol particles, Atmos. Environ., 198, 83–88,
1081   https://doi.org/10.1016/j.atmosenv.2018.10.047, 2019.
1082
1083   Zielinski, T., Bolzacchini, E., Cataldi, M., Ferrero, L., Graßl, S., Hansen, G., Mateos, D., Mazzola, M., Neuber, R., Pakszys,
1084   P., Posyniak, M., Ritter, C., Severi, M., Sobolewski, P., Traversi, R., and Velasco-Merino, C.: Study of chemical and optical
1085   properties of biomass burning aerosols during long-range transport events toward the Arctic in summer 2017, Atmosphere, 11,
1086   84, https://doi.org/10.3390/atmos11010084, 2020.

1087 **Table 1**. List of reactions involving reactive species relevant to this study.

No.	Reactions	References
1	$NO_3^- + hv \rightarrow {}^\bullet NO_2 + O^-$; $\phi = 0.01$	Vione et al., 2006; Benedict et al., 2017
2	$O^- + H_3O^+ \leftrightarrow {}^\bullet OH + H_2O$	
3	$NO_3^- + hv \rightarrow NO_2^- + O(^3P)$; $\phi = 0.011$	
4	$NO_2^- + {}^\bullet OH \rightarrow {}^\bullet NO_2 + OH^-$ ($k = 1.0 \times 10^{10}$ M^{-1} s^{-1})	Mack and Bolton, 1999; Pang et al., 2019a
5	$O_2^{\bullet-} + NO_2^- + 2H^+ \rightarrow {}^\bullet NO_2 + H_2O_2$	Vione et al., 2001; Pang et al., 2019a
6	$NO_2^- + hv \rightarrow {}^\bullet NO + O^-$; $\phi_{OH,300} = 6.7 (\pm 0.9)\%$	Fischer and Warneck, 1996; Mack and Bolton, 1999; Pang et al., 2019a
7	${}^\bullet NO + O_2 \leftrightarrow {}^\bullet ONOO$	Goldstein and Czapski, 1995; Pang et al., 2019a
8	${}^\bullet ONOO + {}^\bullet NO \rightarrow ONOONO$	
9	$ONOONO \rightarrow 2{}^\bullet NO_2$	
10	$HNO_2 + {}^\bullet OH \rightarrow {}^\bullet NO_2 + H_2O$ ($k = 2.6 \times 10^9$ M^{-1} s^{-1})	Kim et al., 2014; Pang et al., 2019a

1088
1089
1090
1091
1092
1093
1094
1095
1096
1097
1098
1099
1100
1101
1102
1103
1104
1105
1106
1107
1108
1109
1110
1111
1112
1113
1114
1115
1116

1117 **Table 2.** Reaction conditions, initial VL (and GUA) decay rate constants, normalized abundance of products, and average
1118 carbon oxidation state (<OS_c>) in each experiment. Except where noted, the reaction systems consisted of VL (0.1 mM); GUA
1119 (0.1 mM), AN (1 mM); SN (1 mM) under air-saturated conditions after 6 h of simulated sunlight irradiation. Analyses were
1120 performed using UHPLC-qToF-MS equipped with an ESI source and operated in the positive ion mode.

Exp no.	pH	Reaction conditions	Initial VL (and GUA) decay rate constants (min^{-1})[b]	Ratio of 50 most abundant products to total products[c]	Normalized abundance of products[d]	Normalized abundance of N-containing compounds[d]	<OS_c>[e] (OS_c of VL: -0.25; OS_c of GUA: -0.57)
A1		VL*	$2.0 \times 10^{-2} \pm 5.8 \times 10^{-5}$	0.59	1.7 ± 0.16	N/A	-0.05
A2	2.5	VL+AN	$1.7 \times 10^{-2} \pm 7.3 \times 10^{-4}$	0.63	1.4 ± 0.19	5.3×10^{-2}	-0.04
A3		VL*	$1.5 \times 10^{-2} \pm 4.2 \times 10^{-4}$	0.53	1.9 ± 0.33	N/A	-0.04
A4	3	VL+AN	$1.5 \times 10^{-2} \pm 2.3 \times 10^{-4}$	0.56	1.9 ± 0.30	3.6×10^{-2}	-0.05
A5		VL*	$1.2 \times 10^{-2} \pm 5.9 \times 10^{-4}$	0.58	0.26 ± 0.42	N/A	-0.16
A6		VL* (N$_2$-saturated)	$3.2 \times 10^{-3} \pm 1.1 \times 10^{-3}$	0.96	$4.7 \times 10^{-2} \pm 0.0027$	N/A	-0.24
A7		VL+AN	$1.2 \times 10^{-2} \pm 8.8 \times 10^{-4}$	0.53	0.37 ± 0.38	1.7×10^{-2}	-0.13
A8		VL+AN (N$_2$-saturated)	$1.9 \times 10^{-3} \pm 9.2 \times 10^{-5}$	0.89	0.12 ± 0.0095	6.3×10^{-3}	-0.21
A9		VL+SN	$1.3 \times 10^{-2} \pm 3.5 \times 10^{-4}$	0.51	0.42 ± 0.33	1.7×10^{-2}	-0.07
A10	4	VL* (0.01 mM)[a]	N/A	0.90	0.37 ± 0.018	N/A	-0.07
A11		VL (0.01 mM) + AN (0.01 mM)	N/A	0.77	0.40 ± 0.074	8.6×10^{-3}	0.12
A12		VL (0.01 mM) + AN	N/A	0.42	0.45 ± 0.025	1.2×10^{-2}	-0.06
A13		GUA only	$6.2 \times 10^{-3} \pm 2.5 \times 10^{-4}$	0.77	N/A	N/A	-0.28
A14		GUA+VL	GUA: $1.4 \times 10^{-2} \pm 4.0 \times 10^{-4}$ VL: $4.3 \times 10^{-3} \pm 2.2 \times 10^{-4}$	0.60	2.2 ± 0.47	N/A	-0.27

1121
1122
1123 [a]Irradiation time for VL* (0.01 mM, A10) was 3 h. [b]The data fitting was performed in the initial linear region. Each value is
1124 the average of results from triplicate experiments. Errors represent one standard deviation. Kinetic measurements were not
1125 performed for experiments marked with N/A. [c]Ratio of the normalized abundance of the 50 most abundant products to that of
1126 total products, except for direct GUA photodegradation and GUA+VL (A13–14) whose ratios are based on the absolute signals
1127 of products. [d]The normalized abundance of products was calculated using Eq. 2. The samples for experiments without nitrate
1128 (marked with N/A) were not analyzed for N-containing compounds. For the GUA experiments, the normalized abundance of
1129 products was calculated only for GUA+VL as the GUA signal from the UHPLC-qToF-MS in the positive ion mode was weak,
1130 which may introduce large uncertainties during normalization. [e]<OS_c> of the 50 most abundant products.

1131
1132
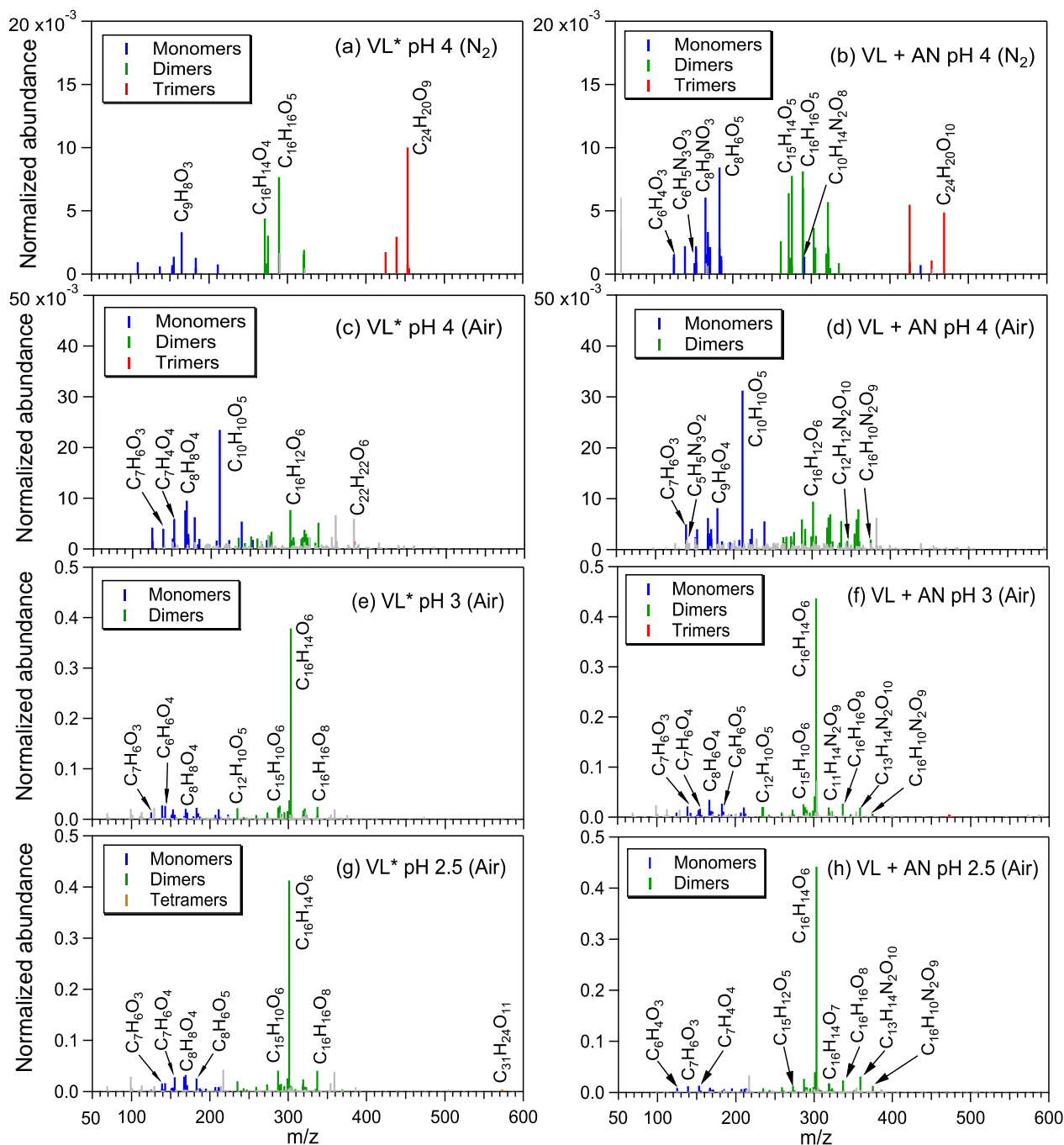
1133

Figure 1. Reconstructed mass spectra of assigned peaks from (a) VL* pH 4 (N₂-saturated; A6), (b) VL+AN pH 4 (N₂-saturated; A8), (c) VL* pH 4 (air-saturated; A5), (d) VL+AN pH 4 (air-saturated; A7), (e) VL* pH 3 (air-saturated; A3), (f) VL+AN pH 3 (air-saturated; A4), (g) VL* pH 2.5 (air-saturated; A1), and (h) VL+AN pH 2.5 (air-saturated; A2) after 6 h of simulated

1137 sunlight irradiation. The normalized abundance of products was calculated using Eq. 2. The 50 most abundant products
1138 contributed more than half of the total normalized abundance of products, and they were identified as monomers (blue), dimers
1139 (green), trimers (red), and tetramers (orange). Grey peaks denote peaks with low abundance or unassigned formula. Examples
1140 of high-intensity peaks were labeled with the corresponding neutral formulas. Note the different scales on the y-axes.

1141

1142

1143

1144

1145

1146

1147

1148

1149

1150

1151

1152

1153

1154

1155

1156

1157

1158

1159
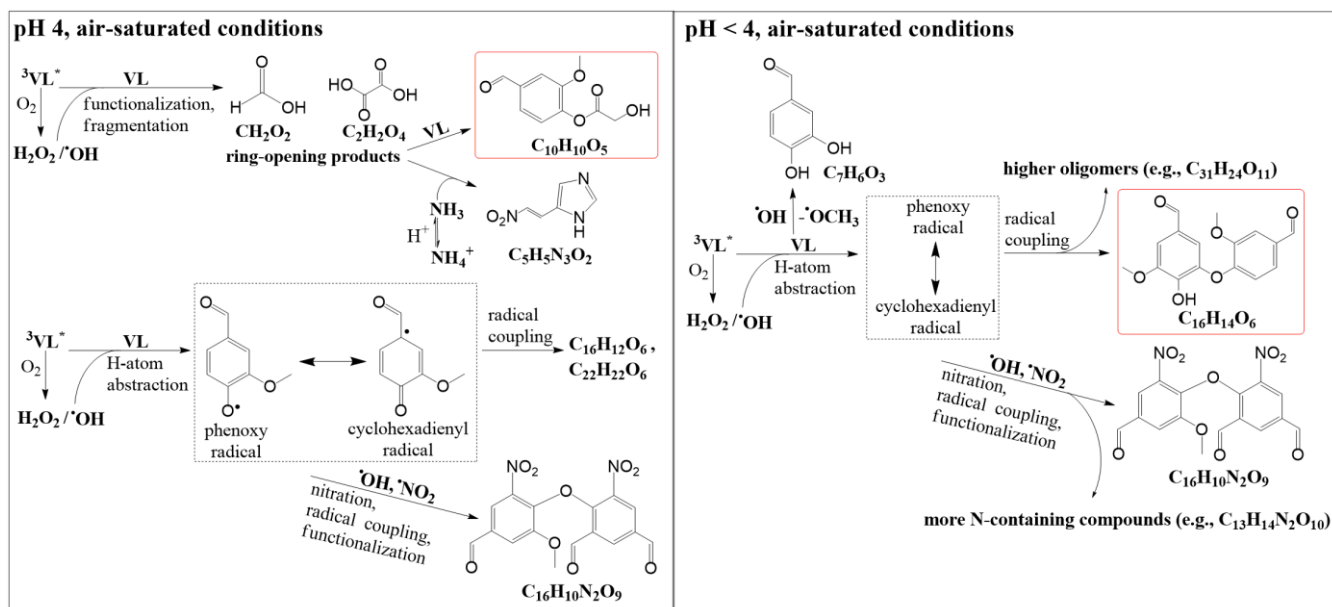
1160

1161 **Figure 2.** Potential aqSOA formation pathways via the direct photosensitized oxidation of VL in the absence (VL*) and
1162 presence of ammonium nitrate (VL+AN) at pH 4 and pH < 4 under air-saturated conditions. Product structures were proposed
1163 based on the molecular formulas, DBE values, and MS/MS fragmentation patterns. The structures presented were the major
1164 products detected using UHPLC-qToF-MS in positive ESI mode. The highlighted structures are the most abundant product
1165 for each condition.

1166

1167

1168

1169

1170

1171

1172

1173

1174

1175

1176

1177

1178
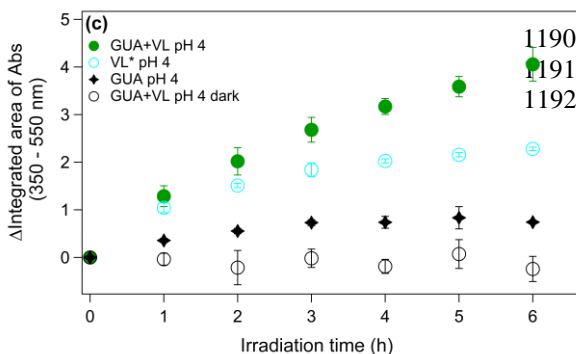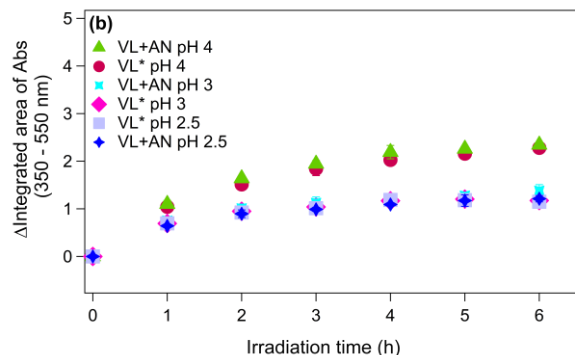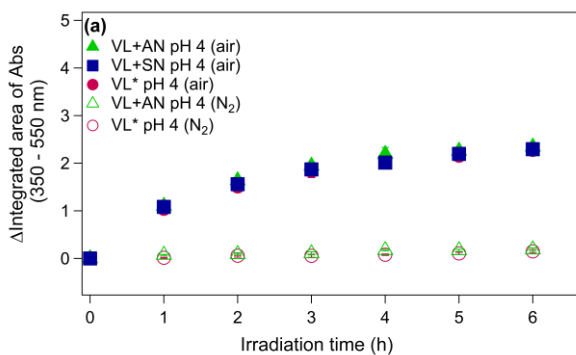
Figure 3. (a–c) Increase in light absorption under different experimental conditions for direct photosensitized oxidation of VL in the absence (VL*) and presence of ammonium nitrate (VL+AN): (a) VL* and VL+AN at pH 4 under N_2- (A6, A8) and air-saturated (A5, A7) conditions. Direct photosensitized oxidation of VL in the presence of sodium nitrate (VL+SN) at pH 4 under air-saturated condition (A9). (b) Effect of pH on VL* and VL+AN at pH 2.5 (A1, A2), 3 (A3, A4), and 4 (A5, A7) under air-saturated conditions. (c) Increase in light absorption during direct GUA photodegradation (A13) and oxidation of GUA via photosensitized reactions of VL (GUA+VL; A14) at pH 4 under air-saturated conditions after 6 h of simulated sunlight irradiation. Error bars represent one standard deviation; most error bars are smaller than the markers.

1234
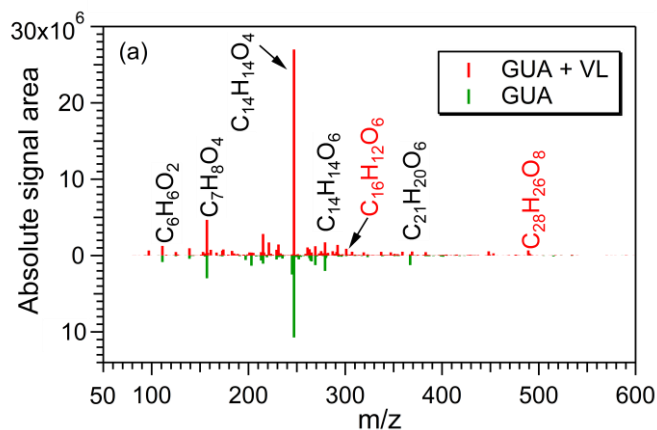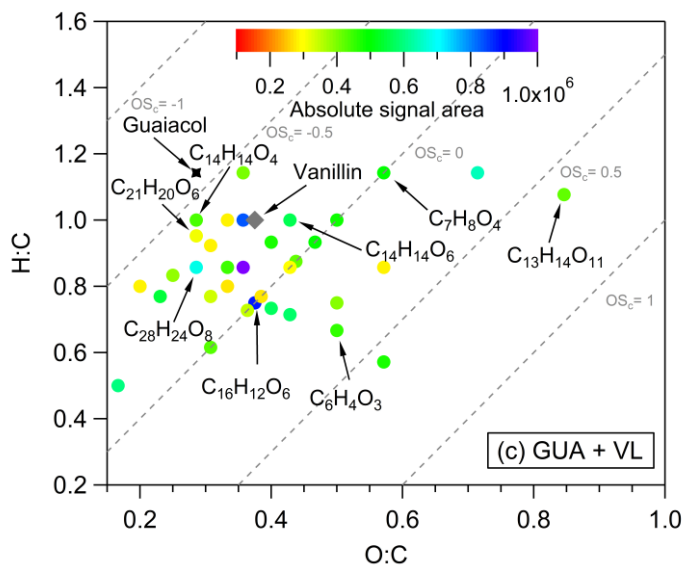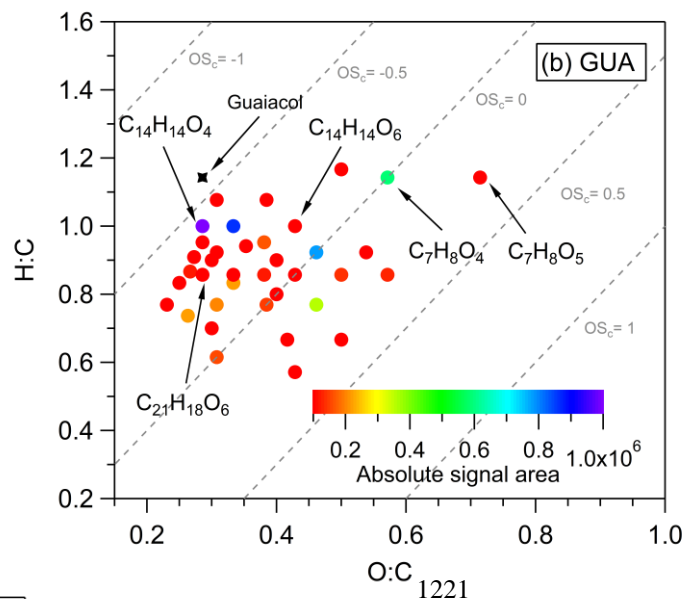
Figure 4. (a) Reconstructed mass spectra of assigned peaks from the direct GUA photodegradation (A13) and oxidation of GUA via photosensitized reactions of VL (GUA+VL; A14) at pH 4 under air-saturated conditions after 6 h of simulated sunlight irradiation. The y-axis is the absolute signal area of the products. Examples of high-intensity peaks were labeled with the corresponding neutral formulas. The formulas in red text correspond to products observed only from GUA+VL. (b-c) van Krevelen diagrams of the 50 most abundant products from the (b) direct photodegradation of GUA (A13) and (c) GUA+VL (A14) at pH 4 under air-saturated conditions after 6 h of simulated sunlight irradiation. The color bar denotes the absolute signal area. The grey dashed lines indicate the carbon oxidation state values (e.g., OS_c =-1, 0, and 1).